Analysis of the transcriptome and metabolome of pancreatic spheroids derived from human induced pluripotent stem cells and matured in an organ-on-a-chip

Amal Essaouiba, Rachid Jellali, Stéphane Poulain, Fumiya Tokito, Françoise Gilard, Bertrand Gakière, Soo Hyeon Kim, Cécile Legallais, Yasuyuki Sakai, Eric Leclerc

Analysis of the transcriptome and metabolome of pancreatic spheroids derived from human induced pluripotent stem cells and matured in organ-on-chip

Amal Essaouiba[1,2,3], Rachid Jellali[1*], Stéphane Poulain[4], Fumiya Tokito[3], Françoise Gilard[5], Bertrand Gakière[5], Soo Hyeon Kim[4], Cécile Legallais[1], Yasuyuki Sakai[2,3], Eric Leclerc[1,2*]

[1] *Université de technologie de Compiègne, CNRS, Biomechanics and Bioengineering, Centre de recherche Royallieu CS 60319, 60203 Compiegne, France.*

[2] *CNRS IRL 2820; Laboratory for Integrated Micro Mechatronic Systems, Institute of Industrial Science, University of Tokyo; 4-6-1 Komaba; Meguro-ku; Tokyo, 153-8505, Japan.*

[3] *Department of Chemical System Engineering, graduate school of Engineering, the University of Tokyo, 7-3-1, Hongo, Bunkyo-ku, Tokyo, 113-8656, Japan.*

[4] *Institute of Industrial Science, The University of Tokyo, 4-6-1 Komaba; Meguro-ku; Tokyo, 153-8505, Japan.*

[5] *Plateforme Métabolisme-Métabolome, Institute of Plant Sciences Paris-Saclay (IPS2), Université Paris-Saclay, CNRS, INRAE, Université d'Evry, Université de Paris, 91190 Gif-sur-Yvette, France*

* corresponding authors:

rachid.jellali@utc.fr

eleclerc@iis.u-tokyo.ac.jp

Abstract

Functional differentiation of pancreatic like tissue from human induced pluripotent stem cells is one of the emerging strategies to achieve *in vitro* pancreas model. Here, we propose a protocol to cultivate hiPSCs-derived β-like-cells coupling spheroids and microfluidic technologies to improve the pancreatic lineage maturation. The protocol led to the development of spheroids producing C-peptide and containing cells positive to insulin and glucagon. In order to further characterize the cellular and molecular profiles, we performed full transcriptomics and metabolomics analysis. The omics analysis confirmed the activation of key transcription factors together with the upregulation of genes and the presence of metabolites involved in functional pancreatic tissue development, extra cellular matrix remodeling, lipids and fatty acids metabolism, and endocrine hormones signaling. When compared to static 3D honeycombs cultures, dynamic 3D biochip cultures contributed to increase specifically the activity of HIF transcription factor, to activate the Calcium Activated Cation Channels, to enrich the glucagon and insulin pathways, glycolysis/gluconeogenesis, and to increase the secretion of serotonin, glycerol and glycerol-3-phosphate at the metabolic levels.

1. Introduction

Diabetes mellitus is one of the major diseases with an increasing prevalence about to reach the epidemic levels. This disorder of the endocrine system of the pancreas affected more than 537 million people worldwide in 2021.[1] Type 1 diabetes mellitus (T1DM) is caused by an autoimmune response leading to the destruction of β-cells producing the insulin.[2] Up to date, T1DM cannot be prevented, and the exact causes of the onset of the disease are still unclear. Type 2 diabetes mellitus (T2DM) generally consists of an insulin resistance and impaired insulin secretion leading to a high level of blood glucose.[3] T2DM can be partially prevented by the modification of the lifestyle with physical activity and healthy food intakes. Besides, diabetes also contributes to increase the risk factors of systemic disorders such as cardiovascular disease and kidney failure.[4]

Cell therapy of T1DM relies on the grafting of pancreas islets of Langerhans harvested from donors. The islets are prepared in the laboratory and then injected in patient's liver where they are stored to regulate the glycemia and the insulin production.[2,5] However, the limitations of this therapy are multiple. Essentially, there is an observed lack and scarcity of donors (about 2 to 3 pancreases are required for one patient). In addition, long term studies have reported transplant degradation and graft loss over time.[5] Moreover, those grafts are coupled with complex and constraining medical treatments due to the patients' immune response to external tissues.[6] To solve those issues, researchers are now developing new solutions to produce islets suitable for implantation in combination with improved strategies to protect the transplants.

Especially, new cell sources and organoids-like-islets production technologies are being developed as stem cell therapy for T1DM.[7] Indeed, pancreatic organoids derived from human induced pluripotent stem cells (hiPSCs) or embryonic stem cells represents one of the strategies proposed in the last decade to provide alternative cell sources to human primary cells.[8-13] However, the development of human equivalent tissue with similar level of functionalities is yet to be achieved in order to propose efficient therapeutic solutions.[7,10,14]

In parallel, several groups also developed engineering solutions to improve the quality of the islets prior to their implantation. It mostly relies on the upstream screening of the islets to evaluate their functionality and performance, and thus enhance the selection process before the injection.[15-17] Additionally, alternative preparation methods also include islets encapsulation to protect the graft from patient's immune system.[18] In recent years, the use of microfluidic technologies in diabetes research has increased remarkably. Due to its many advantages, such as versatility, precise control of volume, size and flow, enhanced efficiency, automation, real-time readout, as well as the creation of well-defined microenvironments, microfluidic technology represents a valuable tool for a wide range of applications related to pancreatic islets and β-cells. This technology can be used for islets and β-cells encapsulation before transplantation,[19,20] pseudo-islets formations from isolated β-cells,[21] islets evaluation and preservation,[22] study of islets physiology and drug screening [23,24] and hiPSCs differentiation into pancreatic β-cells.[25]

Following those technology developments, we have established a culture protocol inside the microfluidic biochips using rat islets of Langerhans. We showed that the microfluidic culture environment contributed to maintain the functionality of the islets in term of insulin and glucagon secretion, when compared to static cultures.[26] Furthermore, this microfluidic culture protocol was extended to culture of β-cells spheroids derived from hiPSCs.[27] We demonstrated that hiPSC-derived spheroids were able to produce insulin and C-peptide. Although the spheroids prepared with our protocol are made of hiPSCs differentiated to pancreatic β-like cells, we noticed that the differentiation process also generated glucagon positive cells. To increase the knowledge on those spheroids, we propose here to extend their characterization by analyzing their transcriptomics and metabolomics profiles.

2. Material and methods

2.1. β-cell spheroids formation using honeycomb technology

The hiPSCs derived β-cells were purchased from Takara Bio (Japan). The cells were previously differentiated from ChiPSC12 line by Takara Bio and provided cryopreserved in

stage 1 of maturation (Fig.1A). In this second stage of maturation (total of 16 days), we used the media kit supplied with the cells (cat. N° Y10108, Takara Bio, Japan), according to the manufacturer's instructions (Fig.1A).

The spheroids were formed using a polydimethylsiloxane (PDMS) honeycomb sheet inserted into a bottomless 24-well plate (Fig.S1, supplementary file 1 and fabrication process in supplementary file 2). The 3D honeycomb technology was developed by Shinohara et al., and has also been described in detail in previous works.[27,28] Before cell seeding, the honeycomb plates were sterilized with ethanol (1 hour) and coated with pluronic acid (Pluronic® F-127 Sigma, 10 mg/mL) dissolved in phosphate-buffered saline (PBS, Gibco) overnight to prevent cell attachment. Then, the plates were rinsed three times with PBS and once with maintenance culture medium (β-cell basal medium Y10104, supplemented with β-cell supplement Y10102). After thawing, $6x10^5$ β-cells in 500 µL of maintenance culture medium were seeded into each well of the honeycomb plate and the plate was incubated at 37°C in an atmosphere supplied with 5% CO_2 for 4 days. After 24h, the total volume of medium was adjusted to 1 mL. We then removed 600 µL at each culture medium change (every day), replacing it with 600 µL of fresh medium (thus resulting in there always being 400 µL of medium remaining in the honeycombs in order to prevent accidental spheroids suction).

2.2. 3D spheroids cultures

2.2.1. 3D static culture in honeycomb plates

After spheroid formation resulting from 4 days of culture in the honeycombs, the β-cell spheroids were collected and seeded in a new honeycomb plate at a density of approximately 200±50 spheroids/well (Fig.1A). The volume of culture medium was adjusted to 1 mL and exchanged every day as described in section 2.1. The maintenance culture medium was used for 8 additional days (day 12 of culture). The assay medium (β-cell medium-2 Y10105, supplemented with β-cell supplement Y10102) was then used from day 12 to day 15 (end of experiments at day 16 of stage 2, Fig.1A).

2.2.2. 3D dynamic culture in biochips manufactures

The biochip fabrication and design details are provided in Essaouiba et al., 2021.[27] The biochip consists of two PDMS layer manufactured using soft lithography and sealed by plasma treatment. For spheroids trapping, the biochip bottom layer contains a crescent-shaped structures of 600 µm in diameter and 300 µm in height (Fig.S2A, supplementary file 1). For perfusion, the biochips were connected to a perfusion's circuit composed of silicone/Teflon tubing (0.65 mm in diameter), bubble trap (culture medium reservoir) and peristaltic pump (Fig.S2B, supplementary file 1). Before the cell experiments, the biochips, tubing and bubble trap were sterilized by autoclaving and dried in an oven.

For the 3D biochip cultures, the β-cell spheroids formed using the honeycomb plates were collected and seeded into the biochips at a density of approximately 200±50 spheroids/biochip. After seeding, the biochips were incubated at 37°C in a 5% CO_2 supplied incubator for 1h to allow the crescent-shaped structures to trap the spheroids. The biochips were then connected to the perfusion circuit, the entire setup incubated at 37°C in a 5% CO_2 supplied incubator and the perfusion launched at 20 µL/min. The culture medium was changed every two days (2 mL). The maintenance culture medium was used until day 12 of culture and then replaced by assay medium for 4 days (until end of the experiments, Fig.1A).

2.3. RT-qPCR assays

RT-qPCR assays were performed as described previously in Essaouiba et al., 2020.[29] The detailed protocol and primer sequences are given in supplementary file 2. ACTB (β-Actin) was used as the reference gene and hiPSCs in stage 1 of maturation (iPSC-ST1, as shown in Fig. 1A) were used as the reference sample for the normalization of gene expression data.

2.4. Immunostaining

Immunostaining was performed on spheroids fixed in paraformaldehyde 4% and permeabilized with 1% Triton X100 in PBS. Primary antibodies (Table S2, supplementary file 2) diluted in the range recommended by the manufacturer were incubated with corresponding samples overnight at 4 °C. After washing, the samples were further incubated with the

secondary antibodies overnight (diluted in the range recommended by the manufacturer, Table S2 in supplementary file 2). The nuclei and actin cytoskeleton were stained with DAPI (342-07431, Dojindo) and phalloidin (Phalloidin-iFluor 488 Reagent, ab176753, Abcam), respectively. The detailed protocol is provided in supplementary file 2

2.5. CAGE transcriptome profiling

The nanoCAGE sequencing libraries generated for this study were prepared as previously described by Poulain et al., 2017.[30] Detailed protocols for total RNA extraction, library preparation, sequencing, and data processing are given in supplementary file 2.

Gene expression tables were created using the CAGEr package[31] and were next uploaded on the iDEP server version 9.1 (http://bioinformatics.sdstate.edu/idep91/) for differential gene expression analysis (limma-voom) and pathway gene set enrichment analysis.[32] The ISMARA web server (https://ismara.unibas.ch/mara/) was used for Motif Activity Response Analysis (MARA) .[33] The Full details of the post processing are given in supplementary file 2.

2.6. Metabolomic analysis

Gas chromatography (Agilent 7890B) coupled to quadrupole mass spectrometry (Agilent 5977A, GC-MS) was used to perform the metabolomic analysis on the culture medium collected from the different culture conditions. Rxi-5SilMS columns (30 m with a 10 m Integra-Guard column, 13623-127, Restek) were used. Preparation of samples and extraction of metabolites were performed according to the protocol previously described.[34] The AMDIS software (http://chemdata.nist.gov/mass-spc/amdis/) was used for data analysis. To consider the difference occurring during the protocols, the data were normalized by the spheroids counted in each biochip and honeycomb, and by the level of metabolite in the basal culture medium. The detailed protocols are given in supplementary file 2.

The MetaboAnalyst 5.0 was used to perform the metabolomic multivariate data analysis.[35] Significant variations between the groups were highlighted by supervised partial least squares-discriminant analysis (PLS-DA). The quality of models was evaluated by the R^2Y (fitting degree) and Q^2 (prediction parameter) values. Differentially expressed metabolites were

identified according to their variable importance for the projection (VIP > 1) and *P* value (Student's t-test, P < 0.05). MetaboAnalyst 5.0 was also used to perform the metabolic pathway analysis using the differentially expressed metabolites.

2.7. Statistical analysis

The experiments were repeated at least three times in triplicate (n = three independant experimental campaigns, each campaign contained at least three 3D Petri and 3D biochip leading to n=3x3=9). For RT-qPCR and metabolomic analysis, 9 replicates (from 3 independent experiments 3x3) were used. Concerning CAGE transcriptome profiling, 6 (from 3 independent experiments 2x3) and 4 (from 3 independent experiments) replicates were used for biochip and Petri conditions, respectively. RT-qPCR data are presented as the mean ± standard deviations (SD). The Kruskal Wallis test was performed to determine any significant differences between the samples (*p*- values < 0.05 were identified as statistically significant).

3. Results

3.1 Morphologies and functional analysis

The iPSC stage 1 cell population was successfully inoculated in the honeycomb and started to form 3D aggregates inside the honeycomb plates as shown in Fig.1B. After 4 days of culture, spheroids were collected from the honeycombs' plates and splitted into two groups. The first group was re-injected in a second set of 3D honeycomb plate (3D Petri) for static controls. The second group of spheroids was inoculated in 3D biochips for dynamic cultures. The spheroids were maintained successfully in culture until the end of the experiments as shown in Figs1C and 1D. The immunostaining of the spheroids in both 3D Petri and in 3D biochips displayed similar patterns as shown in Fig. 2. The spheroids were positive to insulin, glucagon, MAFA, PDX1 and GCK. We did not find any striking difference of the fluorescence intensity between the 3D Petri and 3D biochips conditions.

Typical pancreatic markers were characterized by RT-qPCR (Fig.3). We confirmed that the spheroids in 3D Petri and in 3D biochips over-expressed PDX1, NKX6.1, PTF1A, INS, NKX2.2 and GCK when compared to stage 1 iPSCs. Furthermore, mRNA levels of GLUT2,

GCG and SST were particularly high in 3D Petri when compared to both iPSC-stage 1 cells and 3D biochips. In parallel, we did not find specific upregulation of MAFA, PCSK1 or UCN3, whereas NGN3 gene expression levels appeared downregulated when compared to iPSC-stage 1 cells.

3.2 Transcription factor motif activity response analysis

NanoCAGE transcriptomics data obtained from iPSC-stage 1 cells and the cell samples differentiated either in 3D Petri and in 3D biochip experiments were processed for Motif Activity Response Analysis (MARA) in order to identify important Transcription Factors (TFs) differentially involved in the differentiation process. The overall TFs activity table is given in supplementary file 3. The multivariate analysis performed with this TF motif activity table contributed to separate the 3D biochips, the 3D Petri and the iPSC stage 1 conditions. The heatmap of the top 50 TFs motifs, discriminating the different groups of samples (P value < 0.05), is presented in Fig 4A.

From this analysis, we found that the iPSCs stage 1 was characterized by high activities of the following TFs binding motifs: SOX4, TCF7L2, UCCAGUU, HOXA2_HOXB1, ALX1_ARX, WT1_MTF1_ZBTB7B, UACAGUA, CGUGUCU, KLF7, UUGGUCC, ACUGCAU, ELF_GABA_ELF5, PRRX1_ALX4_PHOX2A, ZIC2_GLI1, SP100 and TFAP2B. In parallel, the 3D Petri was characterized by the increased activity of TFs motifs such as WRNIP1, NROB1, TP63, SOX8, HIC2, FOXK1_FOXP2_FOXB1, RXRG, KLF1 and HIC2. Moreover, 3D biochips were characterized by the enhanced motif activity of HIF1A, AUGGCAC, DDIT3 and SP4_PML. We found that GF11B, ZSCAN4, E2F2_E2F5 and ZNF784 were commonly over activated in iPSC stage 1 and in 3D Petri. Finally, JUN, FOSL1, SOX17, MEF2D_MEF2A, CREB5_CREM_JUNB, BACH1_NFE2_NFE2L2, UAUUGCU and AGUGCUU were commonly over expressed in 3D Petri and 3D Biochips when compared to iPSC-stage 1.

In parallel, the mean motif activity provided by MARA extracted another set of potential interesting transcription factors. NRF1, TBP, GMEB2, HSF4, ZBTB33_CHD2,

ZNF711_TFAP2A_TFAP2D, YY1_YY2, GGAAUGU, MAFB and AIRE were the top 10 active transcription factors with the highest z-value (Fig.4B).

Finally, we extracted a selection of transcription factors from both analysis with potential pancreatic development interest. We plotted the activity profile of NRF1, MAFB, HIF1 and SOX17 (Fig. 4C) as they appeared among the genes with a more activated motif in 3D biochips when compared to 3D Petri and iPSC-stage 1. The regulatory networks of these TFs are provided in Fig.4D and contributed to bridge both set of transcription factors of Figs.4A and 4B. Thus, we found that NRF1 linked with MEF2D_MEF2A gene, MAFB linked with WT1_MTF1_ZBTB7B and HIF1A linked with WRNIP1.

3.3. Transcriptome analysis

3.3.1. Comparison of 3D Petri vs stage 1 iPSC

Transcriptomics data obtained from iPSC-stage 1 and cell samples differentiated in 3D Petri were compared. Differential gene expression analysis was performed with limma-voom in iDEP9.1 with an FDR set at 0.2 and a minimum fold change above 1.1. The analysis led to extract 195 genes differentially expressed between the two conditions (Fig.5A and supplementary file 4). Among the discriminating genes, several lipid-related genes (FABP3, ACAT2, LPIN1, HMGCS1, SQLE), hormones-related genes such as GCG (glucagon), CHGB (Secretogramin B), TTR (transthyretin), INSIG1 (insulin induced gene 1), and receptor KDR (VEGFR) were found upregulated in cells differentiated in the 3D Petri environments. The GO_biological_process gene ontology annotations associated to these upregulated genes confirmed the enrichment of cognate lipid and hormone pathways (Fig.5B). The stage 1 iPSC displayed upregulated gene expressions for FGFR2 and insulin-related genes (IGFBP2, IGF2). Finally, the expression of several ECM-related genes (FN1, ACTB, COL4A5, COL5A2, FLNA) were also found upregulated, leading to an enrichment of the cytoskeletal protein binding GO_molecular_function annotation (Fig.5C).

We next performed pathway analysis using the Gene Set Enrichment Analysis (GSEA) method that considers fold-change values of all genes to identify coherently altered pathways.

The top GO_biological_process pathways identified were related to lipids, steroids and lipoproteins (Fig.S3 and supplementary file 4). These pathways were found over activated in 3D Petri, which corresponds to the upregulation of genes such as HMGCS1, INSIG1, HMGCR, FDFT1, PDK4, PDGFA, FABP3, SQLE, LSS, DKK3, CGA, DHCR7, DHCR24, KPNB1 and ACAT2 (expression levels of selected genes are presented in Fig.5D). Concomitantly, this led to enrichments of the PPAR, Fatty acids and Peroxisome signaling using the GO_KEGG pathway database (Fig.S4 and supplementary file 4). Regarding important GO_molecular_functions, we found that the 3D Petri culture environment contributed to over activate hormone activity through the up regulation of genes such as TTR, COPA, CGA, GCG, INS CHGB and IAPP, together with the down regulation of IGF2 (expression levels of selected genes are displayed in Fig.5D). Other GO_molecular_functions like the lipid processes, amide binding, the iron and sulfur ion functions and the oxidoreductase activity were also found enriched in 3D Petri samples (Fig.S5 and supplementary file 4).

In the stage-1 iPSC, the enriched GO_molecular_functions identified were related to DNA and RNA bindings and methyltransferase activity. We also found an enrichment of the cytoskeleton compounds (Fig.5D). The differences of expression of some ECM related-genes illustrate a balance between the up and down expression of those genes (high expression levels of LAMA1, LAMA2, FN1, COL4A5, COL6A3 and VCAN genes observed in stage 1 iPSC versus high expression levels of COL4A1 and VTN genes measured in 3D Petri, Fig.5D). Finally, the GO_KEGG ECM-receptor pathway was also highlighted (Fig.S4).

3.3.2. Comparison of 3D biochips vs stage 1 iPSC and 3D Petri

The results of the comparison of 3D biochips (at the end of the culture) with the stage 1 iPSC led to identify 418 genes differentially expressed (Fig.S6, the list of genes is given in supplementary file 5). Similarly, to 3D Petri, we found the enrichment of the genes ontologies, using the GSEA formalism, were related to lipids and sterols metabolisms, hormones activity, oxydo-reduction, TCA pathway, glucagon pathway in 3D biochips whereas ECM constituents

were enriched in step 1 iPSC. The details of the enrichments of the GSEA analysis for the biological_process and KEGG pathways are given in Fig.S7 and Fig. S8.

In order to clearly specify the differences between the 3D Petri and the 3D biochips, we performed a dedicated analysis. Differential gene expression analysis was performed with limma-voom in iDEP9.1 with an FDR set at 0.2 and a minimum fold change above 1.1. This led to extract a short list of 112 genes discriminating the two conditions (*nb*: extended to 203 genes with an FDR of 0.3, supplementary file 6). The heatmap showing the top 50 differentially expressed genes is presented in Fig.6A. Among those genes, we found the down regulation of CHGA, INS, TTR (and of VIM, BMP4, FABP3 with FDR <0,3) and the up regulation of FTL, CALR, CHGB, SRC, PRKCD, a protein kinase C, (and of CEBPG, HEXB with FDR < 0,3) in 3D biochip cultures. The gene ontology analysis was performed on the list of those 203 differentially expressed genes. The GO_biological_process and GO_molecular_function annotations found enriched in 3D Petri were related to the response to lipid (overexpression of FABP3, HMGCS1 genes in 3D Petri) and to cytoskeletal constituent (overexpression of ACTB, ACTG1, VIM, NEFM, MAP1B genes in 3D Petri). The 3D dynamic cultures in biochips were characterized by the peptide transport, and various processes linked to the cellular localization (the details of the enrichments are given in supplementary file 6).

To refine the analysis, we further performed pathway analysis by GSEA. The top GO_biological process enriched the negative regulation of stem cell differentiation in 3D Petri whereas we found up regulation of response to angiotensin, positive tissue remolding, gluconeogenesis in 3D biochips as shown in Fig.6B. The GO_molecular function pathways identified in 3D biochips cultures included calcium activated cation channels, GTPase bindings, ubiquitin protein ligase binding, steroid dehydrogenase activity, monosaccharide binding and transferase activity (Fig.6C). TGFβ signaling was identified as the main GO_KEGG pathway overactivated in 3D Petri cultures (Fig.S9), whereas glycolysis/gluconeogenesis, RNA process, insulin pathway and glucagon pathway (Figs.S10 to S13) were overactivated in 3D biochips culture.

3.4 Metabolomic analysis

The GC-MS metabolomic analysis contributed to identify 109 compounds (supplementary file 7). In order to consider the switch in medium after 12 days of culture (in stage 2, see Fig.1A) and the split of islet populations at the biochip inoculation stage (Fig.1A), the metabolites levels were normalized by culture medium levels and the number of islets in each sample.

The multivariate analysis between day 2 (48h in honeycombs during the spheroids formation) and day 16 (the last day of experiment) contributed to distinguishing both time points (PLS-DA score plot in Fig.S14) and extract 20 and 33 metabolites that were differentially expressed in 3D Petri culture with *P values* below 0.05 and 0.1 respectively. The full data including PLS-DA score plot, heatmap and metabolites list (with *P* value and fold change) are provided in Fig.S14 and supplementary file 7. The top 30 of differentially expressed metabolites are displayed in the VIP plot presented in Fig.7A. The signature of 3D Petri cultures at the day 2 included higher levels of fructose, tagatose, lactitol, 2-hydroxybutyrate, methionine sulfoxide, alanine and phenylalanine. The day 16 signature is characterized by higher levels of lipids such as palmitic acid, stearic acid and oleic/elaidic acid.

The same analysis contributed to extract 32 metabolites in 3D biochips that were differentially expressed between day 2 and day 16 with a *P* value below 0.05, and 57 with a *P* value below 0.1 (supplementary file 7). The PLS-DA score plot and heatmap of significantly expressed metabolites are provided in Fig.S15. As shown in the VIP plot of Fig.7B (displaying the top 30 metabolites), the day 2 was characterized by high levels of fructose and adipic acid. At day 16 in 3D biochips, we found high level of several lipids, porphyrin precursor (*nb* in fact the detected compound identified is the 5,10,15,20-tetra(4-pyridyl)-21H,23H-porphine), several glycolysis and carbohydrates substrates and intermediates.

Finally, we directly compared the 3D Petri and the 3D biochips at day 16. The PLS-DA score plot analysis contributed to separate the two conditions with a good predictability and fitting degree (R^2 and $Q^2 > 0.7$, Fig.7C). A total of 21 metabolites with a *P value* below 0.05 (52 with a *P* value below 0.1) were extracted. The list of the metabolites differentially expressed between the two cultures modes is provided in the heatmap in Fig.7C and supplementary file

7. The 3D biochips were characterized by higher levels of glycerol and glycerol-1-phosphate (an intermediate of phospholipids derived from glycerol), whereas 3D Petri led to higher level of glyceric acid (a metabolite of glycerol oxidation), 2 ethyl hexanoic acid (a middle chain long fatty acid), lauric, linoleic and threonic acids. The 3D biochips presented also higher levels of serotonin, lactitol, beta hydroxy isovaleric acid (a hydroxy fatty acid), 2 keto isocaproic acid, pyroglutamate, nicotinamide and picolinic acid.

4. Discussion

Currently, the gold standard in diabetes research and drug screening is the use of primary pancreatic islets of Langerhans. However, the low reproducibility due to different genetic backgrounds, the lake of donors and the variability introduced by the cell collection, cell types and assays, lead to a large variability of the data and thus to bias their interpretation [36]. Furthermore, the limited supply of primary human islets or β-cells remains a major bottleneck in diabetes research and therapy [36]. In that regard, hiPSCs represent a promising alternative and could provide a nearly unlimited number of cells for diabetes studies, anti-diabetic drug development and cell therapies. In addition, to maintain the islets functionality for long-term cultures, to investigate chronic development, it is necessary to understand the intracellular mechanisms of the pathogenesis [37]. Furthermore, to propose new treatments of DM, it is important to understand the human endocrine and exocrine systems, their function and the consequences of their failure [37]. Recently, we have shown that hiPSCs-derived β-cells pseudo-islets cultured in microfluidic biochips display the functions and markers of endocrine pancreas after 2 weeks of culture.[27] In the present study, we confirmed that the spheroids expressed insulin and glucagon (immunostaining) and typical pancreatic genes such as PDX1, NKX6.1, PTF1A, INS, NKX2.2 and GCK. Biomechanical and biochemical stimulations (through shear stress, cell interactions, soluble factors concentrations) largely impact pancreatic islets function and responses.[38] As microfluidic configuration is critical for islet cultures,[39,40] we calibrated our device with rat islets and iPSCs based spheroids in our previous works. Although physiological pancreas islets are exposed to flow rate estimated at 0,03mL/day (estimation of

Sankar et al., 2011 based on the study of Lifson et al., 1985),[40,41] our 20 µL/min flow rate led to a nutrient time residence estimated to 100s. Furthermore, our shear stress of 2 mPa.s is in the range of accepted values beneficial for pancreatic *in vitro* cultures in microfluidic bioreactor (as discussed by Jun et al., 2019).[21]

In order to increase the knowledge of the behaviour on those spheroids maintained in microfluidic biochips, we propose to extend their characterization by full transcriptomics and metabolomics profiling. We analyzed and compared the transcriptome and the metabolome of pancreatic spheroids derived from hiPSCs in honeycombs (3D Petri) and in microfluidic biochips (3D biochips). The transcription factor analysis revealed a difference between the biochip and other conditions (Petri and iPSCs stage 1) through a group of genes with a motif activity related to cell proliferation and pancreas differentiation. The AUGGCAC motif detected in 3D biochips (AUGGCAC associated to MicroRNA-183-5p) is involved in pancreas cancerous cells proliferation.[42] Similarly, we found the over activation in 3D Petri and 3D biochip of MEF2D_MEF2A (MEF2D is linked to cell proliferation in pancreatic tissue).[43] Furthermore, over activated motif AGUGCUU, associated to miR-302c-3p, is normally downregulated during β-cell differentiation in stem cells ,[44] but it was found over activated in our 3D Petri and 3D biochip. In parallel, the transcription factors analysis also reveals the over activation of SOX17 and MAFB motifs in our 3D biochip. That appeared very crucial as far as SOX17 is a key transcriptional regulator that is reported to regulate insulin secretion and prenatal pancreas β-cell function.[45] Furthermore, the maintenance of MAFB is a key point to keep β-cell differentiation.[46] As a result, those data suggest a modulation of the proliferation status and differentiation process of the β-like cells in our model. However, regarding future implantation applications, additional studies would be required to confirm the proliferation capability, especially in link with the inflammation response of the host and the derivation of the spheroids toward tumor like tissue.[47]

The transcriptomic analysis confirmed an important upregulation of genes related to hormones metabolism in the 3D Petri and 3D biochips cultures. We found that TTR, CGA, GCG, CHGB, VGF, IAPP genes (coding for transthyretin, Glycoprotein Hormones Alpha Chain,

glucagon, Chromogranin B, Neuro-Endocrine Specific Protein, Islet Amyloid Polypeptide respectively) were upregulated in spheroids (in 3D Petri and in 3D biochips), when compared to stage 1 iPSCs. It is worth to note that those molecules are important endocrine and pancreatic markers. Thus, TTR is involved in the regulation of Ca^{2+} concentration and insulin release in β-cells.[48] Furthermore, the TTR expression was detected in α-cells that is consistent with our GCG detection.[49] In parallel, islet Amyloid Polypeptide is one of the major β-cell products with a potential role in paracrine islets stimulation and an important player on central nervous system.[50] VGF is a prohormone expressed in neuroendocrine and endocrine tissues. In pancreas it was demonstrated to be a critical node of granule biogenesis in the islet β-cell to coordinate insulin biosynthesis.[51] Consistently CGA regulates vesicles storage and mitochondrial process in insulin secretion.[52] At the metabolome level, the analysis was completed by high level of serotonin, especially in 3D biochips. Serotonin is playing direct action on insulin secretion and in β-cell proliferation.[53] Serotonin is also reported to be produced in β-cells to inhibit α-cells glucagon expression (however, we did not find striking evidence of glucagon lower level in 3D biochips). Furthermore, without serotonin, the regulation of glucagon in α-cells is unpaired during the islets' response to glucose stimulation.[54] Additional intracellular metabolomics analysis (endometabolomics) would provide further information and mechanistic evidence.

At the end of the experiments, the spheroid signatures, both in 3D Petri and 3D biochips were characterized by an important modulation of the lipid signaling when compared to early stage of the differentiation process. Lipids and fatty acids metabolisms are important regulator of the pancreatic functions. Lipid droplets (LDs) accumulation in human pancreatic islets is increased with age.[55] LDs accumulated also in human β-like-cells produced from human embryonic stem cells. Furthermore, LDs accumulation increased in human T2MD islets.[55] In parallel, endogenous uptake of Fatty acid is an important signaling factor in pancreatic β-cells and for insulin secretion.[56] Levels of intracellular glucose also alters the fatty acids metabolism in β-cells.[57] Thus, the lipids exposure and their accumulation are key processes of β-cells dysfunction. Therefore, it is important to understand the relationship between lipids and β-cells

especially in the frame of diabetes therapy [58]. The present metabolomic analysis revealed the high levels of glycerol and glycerol-phosphate in 3D biochips. It is reported that glycerol-3-phosphate formed from glucose are a glycerol source for glycolipids formation in β-cells.[59, 60] Therefore, a metabolic difference was detected at the metabolome levels when comparing 3D Petri and 3D biochips regarding the glycerol metabolism. The production of glycerol-3-phosphate is reported to consume nicotinamide adenine dinucleotide (NADH) and produces NAD^+ that can accelerate the glycolysis. The lipids that are generated, are in turn proposed to promote the insulin secretion.[58] Although we did not quantify the cell number within the spheroid, β-cell proliferation is also regulated by fatty acids which could be another reason of our lipid modulation. Finally, our spheroids contributed to generate glucagon positive tissue in both 3D Petri and 3D biochips (demonstrated from immunostaining). Glucagon is secreted from α-cells and is a paracrine β-cells' regulator.[61] Furthermore, glucagon levels are regulated by fatty acid β-oxidation under low glucose, probably *via* FFAR1 and GPR119.[58]

We may suspect low glucose and oxygen concentrations in the center of the spheroid. In term of disease treatment, HIF is a potential target of anti-diabetic therapy because its inhibition preserves β cell function under metabolic overload [62] (Ilegems et al. 2022). In fact, spheroid's core is largely reported in shortage of nutrients and oxygen.[63] That is consistent with HIF1A over activity found in the transcription factor analysis. Under low glucose, α-cells normally produced glucagon. In addition, under hypoxia, the ratio of α-cells sharply increased inside rat pancreatic islets whereas the β-cells decreased.[64] Furthermore, hypoxia regulated also embryonic pancreatic cells differentiation and insulin-glucagon ratio levels.[65] β-cells derived from embryonic stem cells differentiation appeared regulated under hypoxia by HIF1.[66] HIF is also required to prevent T1DM development.[67] We found high level of GLUT2 mRNA in 3D Petri and 3D biochips (*nb:* 3D Petri > 3D biochips), high level of HIF motif activity in the 3D biochips, INS mRNA higher levels when compared to stage 1 iPSCs (but no statical difference in INS transcriptomic expression in 3D Petri and 3D biochips). Furthermore, we detected higher GCG mRNA level, higher serotonin metabolic production, higher levels of metal ions (ZNF490, ZNF766, FTL), CEPBG (insulin regulator), WDR55 (cell cycle/organogenesis highly

express in pancreas), CHGB (secretory granule genes expressed in α and β cells) and LPER (insulin/glucose homeostasis) at the transcriptomic level that could reflect a specific orientation to the heterogenous α and β lineage differentiation during the 3D differentiation.[68] Finally, a single cell sequencing analysis of human pancreatic islets also demonstrated this type of plasticity of pancreatic tissue with the possibility of de-differentiation between β and α cells.[69] Overall, those literature data are coherent with our 3D Petri and 3D biochip signatures in which both types of β and α cells markers were detected.

Finally, an important difference between 3D Petri and 3D biochip was the larger activation of the TGFβ pathway in 3D Petri (*nb*: nevertheless, the TGFβ pathway is also activated in 3D biochips when compared to stage 1 iPSCs) and the higher level of protein kinase C (PKC) in 3D biochips. TGFβ is a key signaling in the development of pancreas endocrine tissue.[70] More particularly TGFβ1 improves β-cells differentiation, insulin productive cells and insulin release.[71, 72] It is also a key trigger of diabetes in pancreatic cancers [73]. In parallel PKC is reported to play role in islets, ductal and acinar pancreatic cells development, pancreas inflammation and to mediate pancreatic cancer progression.[74] More particularly, PKC proteins required diacylglycerol (a derivate from glycerol-3-phosphate that we found over expressed in 3D biochip metabolome) and calcium binding for their activation (calcium activated ion channel activity is up regulated in 3D biochips when compared to 3D Petri). In β-cells, protein kinase C (PKC), in collaboration with TRPM4 and TRPM5 (*via* GLP1 activation), lead to increase the insulin secretion.[74] While in α-cells, PKCα and PDCδ regulate the glucagon production (*nb*: consistently we found upregulation of PRKCD in 3D biochips).

5. Conclusion

In the present investigation we successfully cultured pancreatic cells in 3D Petri honeycombs and 3D biochips. We have compared the metabolome and transcriptome profiles of spheroids made of induced pluripotent stem derived into β-cells. The spheroids displayed heterogeneous signatures with the expression of α-cells markers such as GCG together with β-cells characteristics such as production of insulin. Glucagon was more expressed in dynamic

cultures, illustrating a potential higher degree of heterogeneity in biochips. The dynamic cultures also contributed to modulate the TGFβ and PKC proteins signaling and HIF-dependent pathway at the gene expression level. The dynamic culture also increased the lipids and serotonin metabolic levels. Finally, we believe that our technology and our approach would be a promising strategy for final application of diabetes therapies, especially considering the insulin and glucagon balance coupled with the transcriptomics related findings due to the clear spheroids' heterogeneity in biochips.

Acknowledgments

A part of this work was supported by French Investissements d'Avenir in the framework of the iLite project (ANR-16-RHUS-0005). The molds used for the fabrication of the PDMS biochips were made by the LAAS in the frame of RENATECH support. Stéphane Poulain was supported by the JSPS Grant-in-aid for Scientific Research (S) 16H06328. We thank the JSPS for its support via the Core to Core program (project JETME). We thank Charles Plessy from OIST, Japan for fruitful discussions in CAGE analysis. Amal Essaouiba received PhD funding from the French Ministry of Higher Education and Research, mobility grants from CNRS/IIS LIMMS IRL 2820 and from the Université de Technologie de Compiegne.

Conflict of interest statement

The authors declare no conflict of interest.

Authors contributions

AE performed the biological experiments, designed the experiments and participated to data analysis and in the writing of the manuscript, RJ performed the metabolomic analysis, contributed to the experimental design and participated to AE supervision and in the writing of the manuscript, SP generated nanoCAGE libraries, processed transcriptomics data and participated in the writing of the manuscript, FT made the honeycomb plates, FG and BG were involved in metabolomics analysis, SHK was involved in the transcriptomics analysis, CL and

YS were involved in the experimental design and AE supervision, EL is the project supervisor, designed the experiments and participated to data analysis and the writing of the manuscript. All authors are involved in the manuscript revision and approval.

References

1 K. Ogurtsova, L. Guariguata, N. C. Barengo, P. L. Ruiz, J. W. Sacre, S. Karuranga, H. Sun, E. J. Boyko and D. J. Magliano, *Diabetes Res. Clin. Pract*., 2022, **183**, 109118.

2 R. Jellali, A. Essaouiba, E. Leclerc and C. Legallais, in *Current Trends and Future Developments on (Bio-) Membranes*, ed. A. Basile, M. C. Annesini, V. Piemonte, C. Charcosset, Elsevier, 2020, chapter 4: Membrane bioreactors for bio-artificial pancreas, 77-108.

3 R. A. DeFronzo, E. Ferrannini, L. Groop, R. R. Henry, W. H. Herman, J. J. Holst, F. B. Hu, C. R. Kahn, I. Raz, G. I. Shulman, D. C. Simonson, M. A. Testa and R. Weiss, *Nat. Rev. Dis. Primers*, 2015, **1**, 15019.

4 J. M. Forbes, and M. E. Cooper, *Physiol. Rev.,* 2013, **93**, 137-188.

5 F. Bertuzzi, L. De Carlis, M. Marazzi, A. G. Rampoldi, M. Bonomo, B. Antonioli, M. C. Tosca, M. Galuzzi, A. Lauterio, D. Fava, P. Dorighet, A. De Gasperi and G. Colussi, *Cell Transplant.*, 2018, **27**, 840-846.

6 Y. Aghazadeh and M. C. Nostro, *Curr. Diab. Rep.,* 2017, **17**, 37.

7 S. Chen, K. Du and C. Zou, *Stem Cell Res. Ther.,* 2020, **11**, 275.

8 M. Hosoya, *Islets*, 2012, **4**, 249-252.

9 S. Zhu, H. A. Russ, X. Wang, M. Zhang, T. Ma, T. Xu, S. Tang, M. Hebrok and S. Ding, *Nat. Commun.*, 2016, **7**, 10080.

10 S. Kahraman, E. R. Okawa and R. N. Kulkarni, *Curr. Diab. Rep.,* 2016, **16**, 70.

11 M. Hohwieler, M. Müller, P. O. Frappart and S. Heller, *Stem Cells Int.*, 2019, **2019**, 9301382.

12 J. R. Millman, C. Xie, A. Van Dervort, M. Gürtler, F. W. Pagliuca and D. A. Melton, *Nat. Commun.*, 2016, **7**, 11463.

13 J. R. Millman and F. W. Pagliuca, *Diabetes*, 2017, **66**, 1111-1120.

14 T. Boettler, D. Schneider, Y. Cheng, K. Kadoya, E. P. Brandon, L. Martinson and M. von Herrath, *Cell Transplant.,* 2016, **25**, 609-614.

15 F. R. Castiello, K. Heileman and M. Tabrizian, *Lab Chip*, 2016, **16**, 409-431.

16 G. Lenguito, D. Chaimov, J. R. Weitz, R. Rodriguez-Diaz, S. A. Rawal, A. Tamayo-Garcia, A. Caicedo, C. L. Stabler, P. Buchwald and A. Agarwal, *Lab chip*, 2017, **17**, 772-781.

17 S H. Lee, S. Hong, J. Song, B. Cho, E. J. Han, S. Kondapavulur, D. Kim and L. P. Lee, *Adv. Healthc. Mater.*, 2018, **7**, 1701111.

18 V. Vaithilingam, S. Bal and B. E. Tuch, *Rev. Diabet. Stud.,* 2017, **14**, 51-78.

19 Y. Jun, M. J. Kim, Y. H. Hwang, E. A. Jeon, A. R. Kang, S. H. Lee and D. Y. Lee, *Biomaterials*, 2013, **34**, 8122-8130.

20 J. D. Weaver, D. M. Headen, M. M. Coronel, M. D. Hunckler, H. Shirwan and A. J. García, *Am. J. Transplant*., 2019, **19**, 1315-1327.

21 Y. Jun, J. Lee, S. Choi, J. H. Yang, M. Sander, S. Chung and S. H. Lee, *Sci. Adv.,* 2019, **5**, eaax4520.

22 S. N. Patel, M. Ishahak, D. Chaimov, A. Velraj, D. LaShoto, D. W. Hagan, P. Buchwald, E. A. Phelps, A. Agarwal and C. L. Stabler, *Sci. Adv*., 2021, **7**, eaba5515.

23 J. F. Dishinger, K. R. Reid and R. T. Kennedy, *Anal. Chem*., 2009, **81**, 3119-3127.

24 P. M. Misun, B. Yesildag, F. Forschler, A. Neelakandhan, N. Rousset, A. Biernath, A. Hierlemann and O. Frey, *Adv. Biosyst*. 2020, **4**, e1900291.

25 K. Hirano, S. Konagaya, A. Turner, Y. Noda, S. Kitamura, H. Kotera and H. Iwata, *Biochem. Biophys. Res. Commun*., 2017, **487**, 344-350.

26 A. Essaouiba, T. Okitsu, R. Jellali, M. Shinohara, M. Danoy, Y. Tauran, C. Legallais, Y. Sakai and E. Leclerc, *Mol. Cell Endocrinol.,* 2020, **514**, 110892.

27 A. Essaouiba, R. Jellali, M. Shinohara, B. Scheidecker, C. Legallais, Y. Sakai and E. Leclerc, *J. Biotechnol.,* 2021, **330**, 45-56.

28 M. Shinohara, H. Kimura, K. Montagne, K. Komori, T. Fujii and Y. Sakai, *Biotechnol. Prog*., **2014**, 30, 178-187.

29 A. Essaouiba, T. Okitsu, R. Kinoshita, R. Jellali, M. Shinohara, M. Danoy, C. Legallais, Y. Sakai and E. Leclerc, *Biochem. Eng. J.,* 2020, **164**, 107783.

30 S. Poulain, S. Kato, O. Arnaud, J. E. Morlighem, M. Suzuki, C. Plessy and M. Harbers, in *Promoter Associated RNA. Methods in Molecular Biology*, ed. S. Napoli, Humana Press, New York, 2020, NanoCAGE: A method for the analysis of coding and noncoding 5′-capped transcriptomes, 57-109.

31 V. Haberle, A. R. Forrest, Y. Hayashizaki, P. Carninci and B. Lenhard, *Nucleic Acids Res.*, 2015, **43**, e51.

32 S. X. Ge, E. W. Son and R. Yao, *BMC Bioinformatics*, 2018, **19**, 534.

33 P. J. Balwierz, M. Pachkov, P. Arnold, A. J. Gruber, M. Zavolan and E. van Nimwegen, *Genome Res.*, 2014, **24**, 869-884.

34 R. Jellali, F. Gilard, V. Pandolfi, A. Legendre, M. J. Fleury, P. Paullier, C. Legallais and E. Leclerc, *J. Appl. Toxicol.,* 2018, **38**, 1121-1134.

35 Z. Pang, J. Chong, G. Zhou, GD. A. de Lima Morais, L. Chang, M. Barrette, C. Gauthier, P. E. Jacques, S. Li and J. Xia, *Nucleic Acids Res.,* 2021, **49**, W388-W396.

36 Hart, N.J., Powers, A.C, . *Diabetologia,* 2019, **62,** 212–222

37 Qadir, M.M.F., Álvarez-Cubela, S., Weitz, J. *et al.*, . *Nat Commun.*, 2020, **11,** 3265

38 R. Tran, C. Moraes and C. Hoesli, *Front. Bioeng. Biotechnol.*, 2020, **8**, 583970.

39 P. N. Silva, B. J. Green, S. M. Altamentova and J. V. Rocheleau, *Lab Chip*, 2013, **13**, 4374-4384.

40 K. S. Sankar, B. J. Green, A. R. Crocker, J. E. Verity, S. M. Altamentova and J. V. Rocheleau, *PloS one*, 2011, **6**, e24904.

41 N. Lifson, C. V. Lassa and P. K. Dixit, *Am. J. Physiol.,* 1985, **249**, E43-E48.

42 F. Miao, J. Zhu, Y. Chen, N. Tang, X. Wang and X. Li, *Oncol. Lett.,* 2016, **11**, 134-140.

43 Z. Song, C. Feng, Y. Lu, Y. Gao, Y. Lin and C. Dong, *Am. J. Transl. Res.*, 2017, **9**, 4836-4847.

44 G. Sebastiani, M. Valentini, G. E. Grieco, G. Ventriglia, L. Nigi, F. Mancarella, S. Pellegrini, G. Martino, V. Sordi, L. Piemonti and F. Dotta, *Acta diabetol.,* 2017, **54**, 265-281.

45 D. Jonatan, J. R. Spence, A. M. Method, M. Kofron, K. Sinagoga, L. Haataja, P. Arvan, G. H. Deutsch and J. M. Wells, *PLoS One*, 2014, **9**, e104675.

46 R. Russell, P. P. Carnese, T. G. Hennings, E. M. Walker, H. A. Russ, J. S. Liu, S. Giacometti, R. Stein and M. Hebrok, *Nat. Commun.*, 2020, **11**, 2742.

47 E. Z. Sim, N. Shiraki and S. Kume, *Inflamm. Regener.,* 2021, **41**, 1.

48 E. Refai, N. Dekki, S. N. Yang, G. Imreh, O. Cabrera, L. Yu, G. Yang, S. Norgren, S. M. Rössner, L. Inverardi, C. Ricordi, G. Olivecrona, M. Andersson, H. Jörnvall, P. O. Berggren and L. Juntti-Berggren, *Proc. Natl. Acad. Sci. USA*, 2005, **102**, 17020-17025.

49 G. T. Westermark and P. Westermark, *Exp. Diabetes Res.,* 2008, **2008**, 429274.

50 P. Westermark, A. Andersson and G.T. Westermark, *Physiol. Rev.*, 2011, **91**, 795-826.

51 S. B. Stephens, R. J. Edwards, M. Sadahiro, W. J. Lin, C. Jiang, S. R. Salton and C. B. Newgard, *Cell Rep.,* 2017, **20**, 2480-2489.

52 J. Wollam, S. Mahata, M. Riopel, A. Hernandez-Carretero and A. Biswas, A., Bandyopadhyay, G.K., Chi, N.W., Eiden, L.E., Mahapatra, N.R., Corti, A., Webster, N., Mahata, *Cell Tissue Res.*, 2017, **368**, 487-501.

53 D. J. Hill, in Diet, nutrition, and fetal programming, ed. R. Rajendram, V. Preedy, V. Patel, Humana Press, New York, 2017, Pancreatic GABA and serotonin actions in the pancreas and fetal programming of metabolism, 529-541.

54 J. Almaça, J. Molina, D. Menegaz, A. N. Pronin, A. Tamayo, V. Slepak, P. O. Berggren and A. Caicedo, *Cell Rep.,* 2016, **17**, 3281-3291.

55 X. Tong, C. Dai, J. T. Walker, G. G. Nair, A. Kennedy, R. M. Carr, M. Hebrok, A. C. Powers and R. Stein, *Diabetes*, 2020, **69**, 342-354.

56 S. Hauke, K. Keutler, P. Phapale, D. A. Yushchenko and C. Schultz, *Diabetes*, 2018, **67**, 1986-1998.

57 G. C. Yaney and B. E. Corkey, *Diabetologia*, 2003, **46**, 1297-1312.

58 Y. Imai, R. S. Cousins, S. Liu, B. M. Phelps and J. A. Promes, *Ann. NY. Acad. Sci.*, 2020, **1461**, 53-72.

59 M. A. Lorenz, M.A. El Azzouny, R. T. Kennedy and C. F. Burant, *J. Biol. Chem.*, 2013, **288**, 10923-10935.

60 M. El-Azzouny, C. R. Evans, M. K. Treutelaar, R. T. Kennedy and C. F. Burant, *J. Biol. Chem.*, 2014, **289**, 13575-13588.

61 R. Rodriguez-Diaz, R. D. Molano, J. R. Weitz, M. H. Abdulreda, D. M. Berman, B. Leibiger, I. B. Leibiger, N. S. Kenyon, C. Ricordi, A. Pileggi, A. Caicedo and P. O. Berggren, *Cell Metab.*, 2018, **27**, 549-558.e4.

62 Ilegems E, Bryzgalova G, Correia J, Yesildag B, Berra E, Ruas JL, Pereira TS, Berggren PO., *Sci Transl Med.*, 2022, **14**, eaba9112.

63 H. Komatsu, F. Kandeel and Y. Mullen, *Pancreas*, 2018, **47**, 533-543.

64 K. Bloch, J. Vennäng, D. Lazard and P. Vardi, *Cell Biol.,* 2012, **137**, 801-810.

65 S. Cechin, S. Alvarez-Cubela, J. A. Giraldo, R. D. Molano, S. Villate, C. Ricordi, A. Pileggi, L. Inverardi, C. A. Fraker and J. Domínguez-Bendala, *Stem Cells Transl. Med.*, 2014, **3**, 277-289.

66 M. Heinis, M. T. Simon, K. Ilc, N. M. Mazure, J. Pouysségur, R. Scharfmann and B. Duvillié, *Diabetes*, 2010, **59**, 662-669.

67 A. Lalwani, J. Warren, D. Liuwantara, W. J. Hawthorne, P. J. O'Connell, F. J. Gonzalez, R. A. Stokes, J. Chen, D. R. Laybutt, M. E. Craig, M. M. Swarbrick, C. King and J. E. Gunton *Cell Rep.*, 2019, **27**, 2370-2384.e6.

68 L. Marroquí, A. Gonzalez, P. Ñeco, E. Caballero-Garrido, E. Vieira, C. Ripoll, A. Nadal and I. Quesada, *J. Mol. Endocrinol.*, 2012, **49**, R9-R17.

69 A. Teo, C. S. Lim, L. F. Cheow, T. Kin, J. A. Shapiro, N. Y. Kang, W. Burkholder and H. H. Lau, *Cell Death Discov.*, 2018, **4**, 14.

70 J. H. Lee, J. H. Lee and S. G. Rane, *Endocrinology*, 2021, **162**, bqaa233.

71 F. Sanvito, P. L. Herrera, J. Huarte, A. Nichols, R. Montesano, L. Orci and J. D. Vassalli, *Development*, 1994, **120**, 3451-3462.

72 Y. Totsuka, M. Tabuchi, I. Kojima, Y. Eto, H. Shibai and E. Ogata, *Biochem. Biophys. Res. Commun.*, 1989, **158,** 1060-1065.

73 Parajuli P, Nguyen, T.L., Prunier C., Razzaque M., Xu K, and Atfi A., *Life Sci Alliance*, 2020, **3**, e201900573.

74 Fleming, A.K., Storz, P., 2017. Protein kinase C isoforms in the normal pancreas and in pancreatic disease. Cellular Signal. 40, 1-9.

Figures captions

Fig.1. Differentiation of hiPSCs in pancreatic β-cells. (A) Chronology of differentiation process from hiPSCs to β-cells. Stage 1 correspond to first stage of differentiation performed by manufacturer (Takara Bio, iPSCs stage 1) and stage 2 correspond to the authors differentiation (maturation) protocols; (B) morphology of the β-cell spheroids formed in the static honeycomb Petri at day 4 of stage 2 of maturation; (C and D) morphology of β-cell spheroids in 3D honeycombs Petri and 3D biochip at day 16 of stage 2 of maturation (end of the experiments), respectively.

Fig.2. iPSC-derived β-cells spheroids characterization at the end of the differentiation (day 16 of stage 2 of maturation) by immunostaining of pancreatic markers: PDX1, GCK, MAFA, glucagon, insulin and DAPI, phalloidin. (A) 3D biochip culture and (B) 3D honeycomb Petri culture (static).

Fig.3. mRNA levels of pancreatic markers in β-cell spheroids at the end of the differentiation (day 16 of stage 2 of maturation) in static 3D Petri and 3D-biochip. The mRNA levels are presented as a ratio between 3D Petri ratio and 3D biochip, and stage1-iPSCs (iPSC-ST1) to highlighted the variation at the end of differentiation compared to immature β-cell (iPSC-ST1).

Fig.4. Comparison of important Transcription Factors (TFs) extracted from NanoCAGE transcriptomics data of β-cell spheroids at the end of the differentiation in static 3D Petri and dynamic 3D-biochip, and immature β-cell (iPSC-ST1). (A) Heatmap of transcription factor motif activities discriminating the 3D Biochip, 3D Petri and iPSC-stage 1 conditions; (B and C) motif activity of selected TFs; (D) regulatory networks of NRF1, MAFB, HIF1A and SOX17 TFs.

Fig.5. Transcriptomics profiling of β-cell spheroids at the end of the differentiation in static 3D Petri and immature β-cell (iPSC-ST1). (A) Heatmap illustrating the transcriptomic separation of the 3D Petri and iPSC-stage 1 conditions; (B, C) GO_biological process and GO_molecular function annotations enriched in 3D Petri and iPSC-stage 1 (the enrichment was performed in iDEP 9.1 using the genes differentially expressed between th two conditions); (D) heatmaps of expression levels of selected genes involved in lipids, hormones and ECM related pathways.

Fig.6. Comparison of the transcriptome profiles of mature (day 16 of stage 2 of maturation) β-cell spheroids differentiated in static 3D Petri and dynamic 3D

biochip. (A) Heatmap of the top 50 genes discriminating the β-cell differentiated in 3D biochip and 3D Petri; (B and C) GO_biological process and GO_molecular function annotations enriched in 3D biochips and 3D Petri (the enrichment was performed in iDEP 9.1 using the genes differentially expressed between the two conditions). Enriched GO annotations in 3D Petri are indicated with green dots, while those enriched in 3D biochips are indicated in red.

Fig.7. Metabolomic signatures of hiPSCs-derived β-cell cultured in 3D Petri and 3D biochip, at different times of stage 2 of maturation. (A) VIP plot discriminating the day 2 and day 16 of culture in 3D Petri; (B) VIP plot discriminating the day 2 and day 16 of culture in 3D Biochip; (C) multivariate statistical analysis comparing β-cell differentiated in 3D Petri and 3D Biochip at the end of the differentiation (day 16 of stage 2 of maturation): PLS-DA score plot separating the two conditions, PLS-DA model validation and heatmap of top metabolites contributing to 3D Petri and 3D biochip cultures separation.

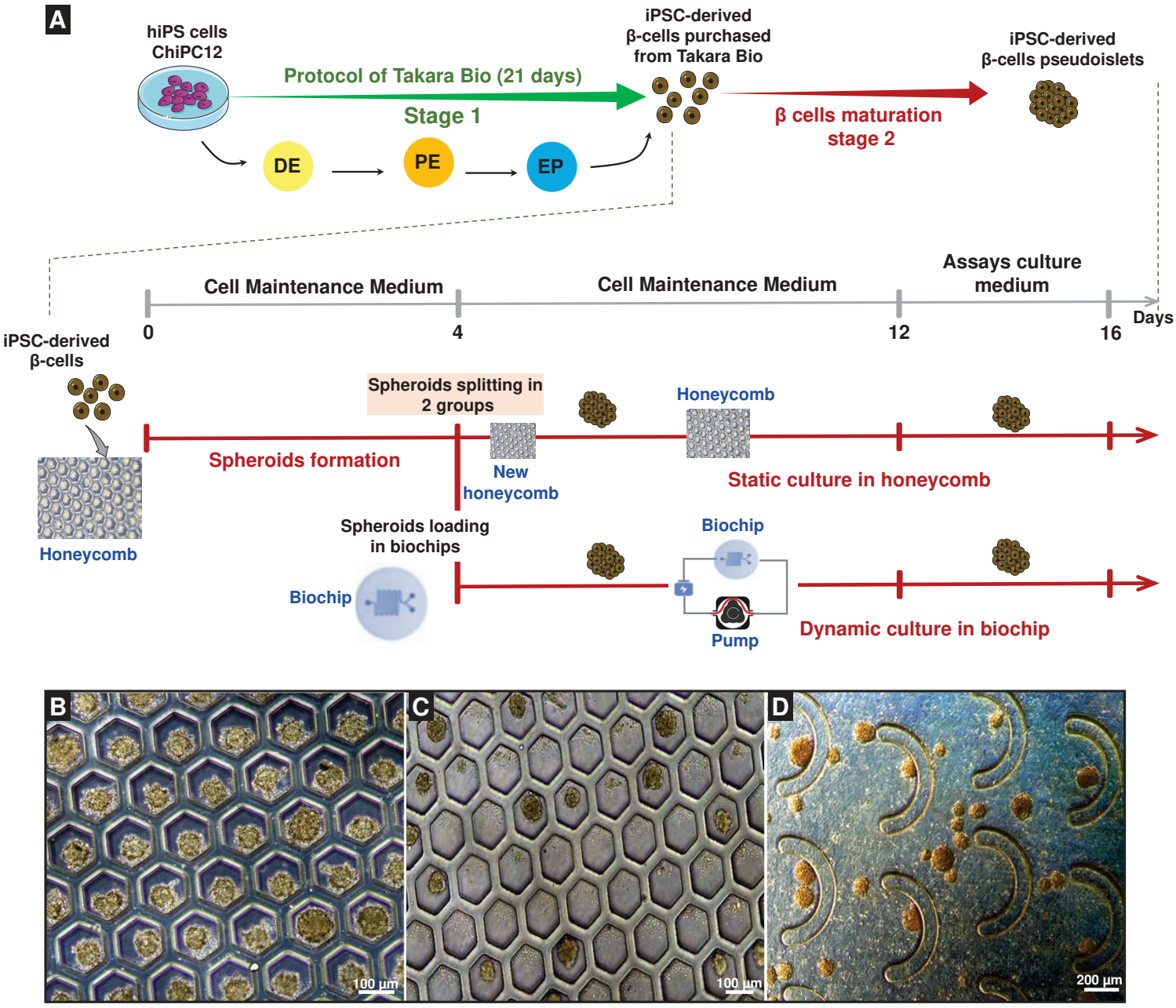
A
hiPS cells
ChiPC12
Protocol of Takara Bio (21 days)
Stage 1
DE
PE
EP
iPSC-derived
β-cells purchased
from Takara Bio
β cells maturation
stage 2
iPSC-derived
β-cells pseudoislets
Cell Maintenance Medium
Cell Maintenance Medium
Assays culture
medium
0
4
12
16
Days
iPSC-derived
β-cells
Honeycomb
Spheroids formation
Spheroids splitting in
2 groups
New
honeycomb
Honeycomb
Static culture in honeycomb
Spheroids loading
in biochips
Biochip
Biochip
Pump
Dynamic culture in biochip

B
100 µm
C
100 µm
D
200 µm

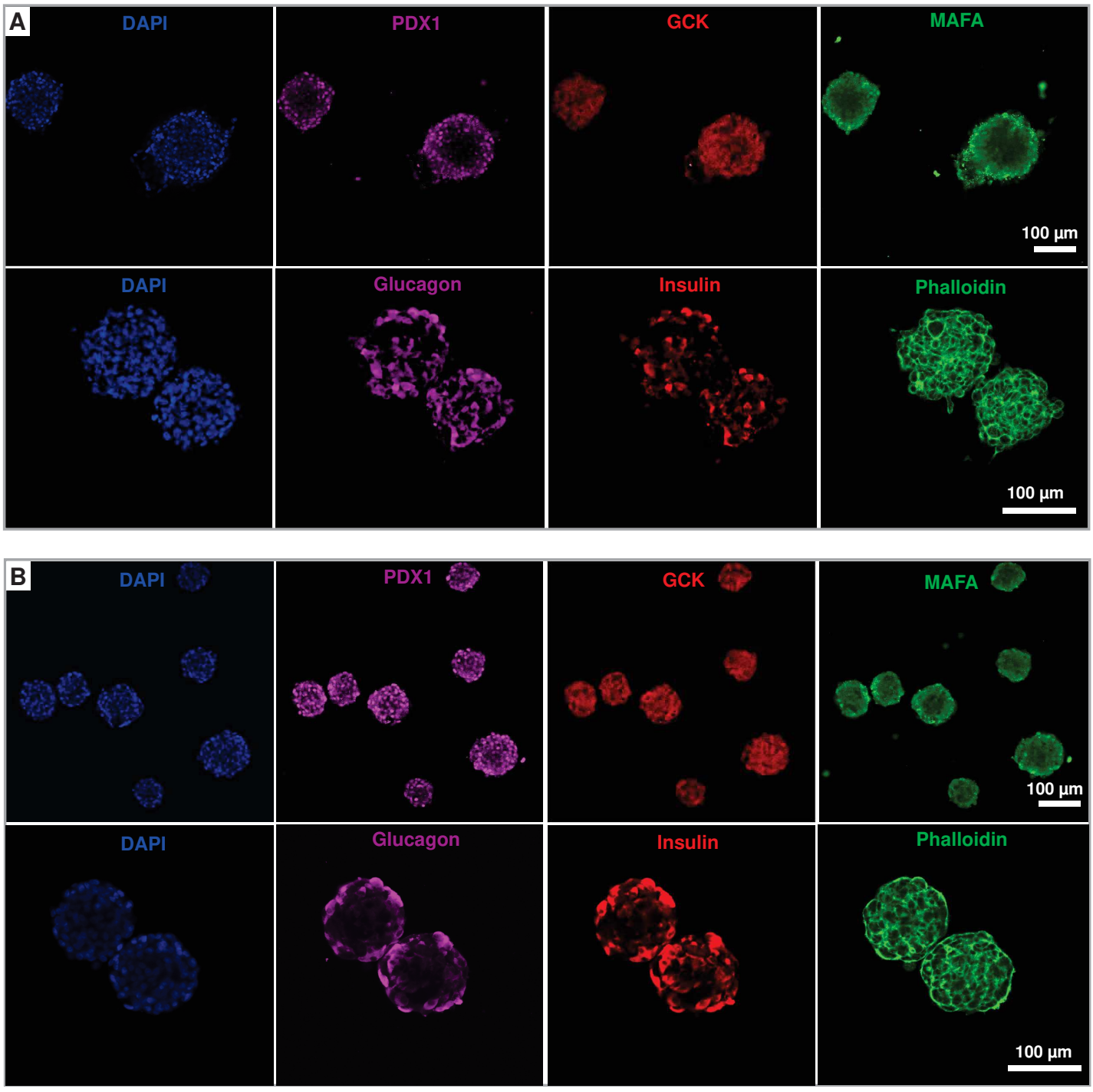
A
DAPI
PDX1
GCK
MAFA
100 μm
DAPI
Glucagon
Insulin
Phalloidin
100 μm
B
DAPI
PDX1
GCK
MAFA
100 μm
DAPI
Glucagon
Insulin
Phalloidin
100 μm

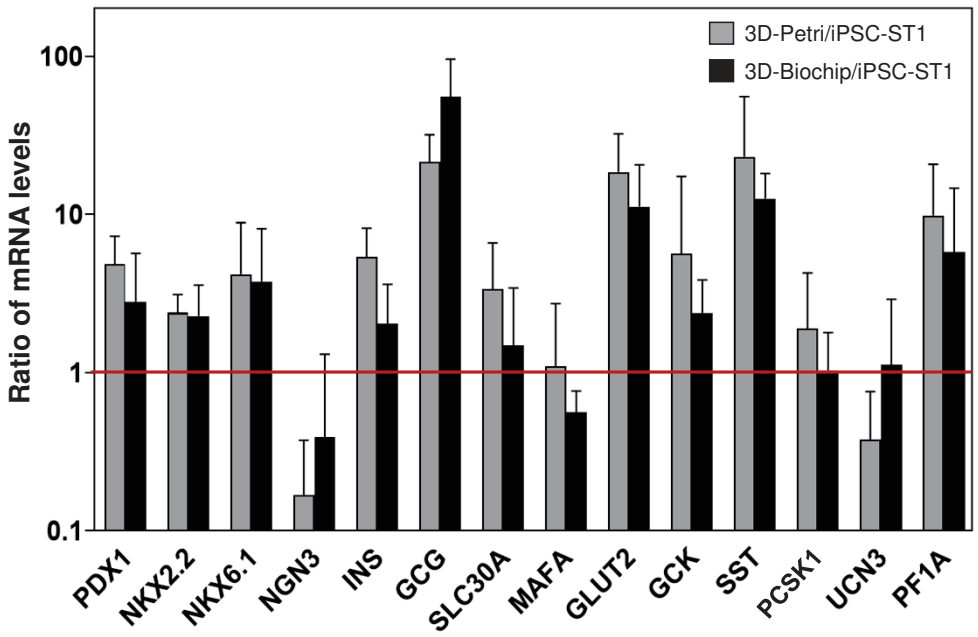
3D-Petri/iPSC-ST1
3D-Biochip/iPSC-ST1
Ratio of mRNA levels
100
10
1
0.1
PDX1
NKX2.2
NKX6.1
NGN3
INS
GCG
SLC30A
MAFA
GLUT2
GCK
SST
PCSK1
UCN3
PF1A

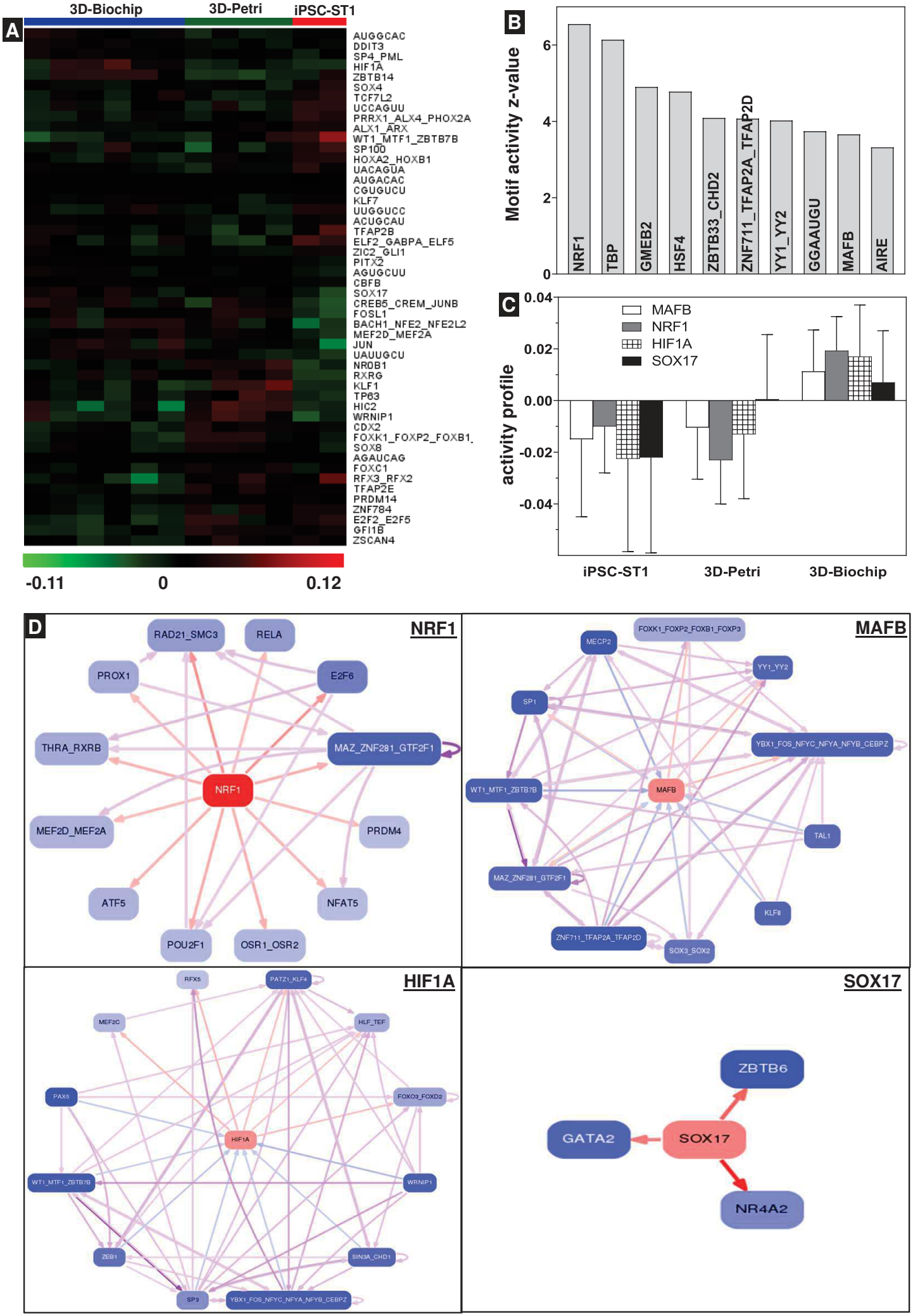
A
3D-Biochip
3D-Petri
iPSC-ST1
AUGGCAC
DDIT3
SP4_PML
HIF1A
ZBTB14
SOX4
TCF7L2
UCCAGUU
PRRX1_ALX4_PHOX2A
ALX1_ARX
WT1_MTF1_ZBTB7B
SP100
HOXA2_HOXB1
UACAGUA
AUGACAC
CGUGUCU
KLF7
UUGGUCC
ACUGCAU
TFAP2B
ELF2_GABPA_ELF5
ZIC2_GLI1
PITX2
AGUGCUU
CBFB
SOX17
CREB5_CREM_JUNB
FOSL1
BACH1_NFE2_NFE2L2
MEF2D_MEF2A
JUN
UAUUGCU
NR0B1
RXRG
KLF1
TP63
HIC2
WRNIP1
CDX2
FOXK1_FOXP2_FOXB1_
SOX8
AGAUCAG
FOXC1
RFX3_RFX2
TFAP2E
PRDM14
ZNF784
E2F2_E2F5
GFI1B
ZSCAN4
-0.11
0
0.12
B
Motif activity z-value
6
4
2
0
NRF1
TBP
GMEB2
HSF4
ZBTB33_CHD2
ZNF711_TFAP2A_TFAP2D
YY1_YY2
GGAAUGU
MAFB
AIRE
C
activity profile
0.04
0.02
0.00
-0.02
-0.04
MAFB
NRF1
HIF1A
SOX17
iPSC-ST1
3D-Petri
3D-Biochip
D
NRF1
RAD21_SMC3
RELA
PROX1
E2F6
THRA_RXRB
MAZ_ZNF281_GTF2F1
NRF1
MEF2D_MEF2A
PRDM4
ATF5
NFAT5
POU2F1
OSR1_OSR2
MAFB
FOXK1_FOXP2_FOXB1_FOXP3
MECP2
YY1_YY2
SP1
YBX1_FOS_NFYC_NFYA_NFYB_CEBPZ
WT1_MTF1_ZBTB7B
MAFB
TAL1
MAZ_ZNF281_GTF2F1
KLF8
ZNF711_TFAP2A_TFAP2D
SOX3_SOX2
HIF1A
RFX5
PATZ1_KLF4
MEF2C
HLF_TEF
PAX5
FOXO3_FOXD2
HIF1A
WT1_MTF1_ZBTB7B
WRNIP1
ZEB1
SIN3A_CHD1
SP3
YBX1_FOS_NFYC_NFYA_NFYB_CEBPZ
SOX17
ZBTB6
GATA2
SOX17
NR4A2

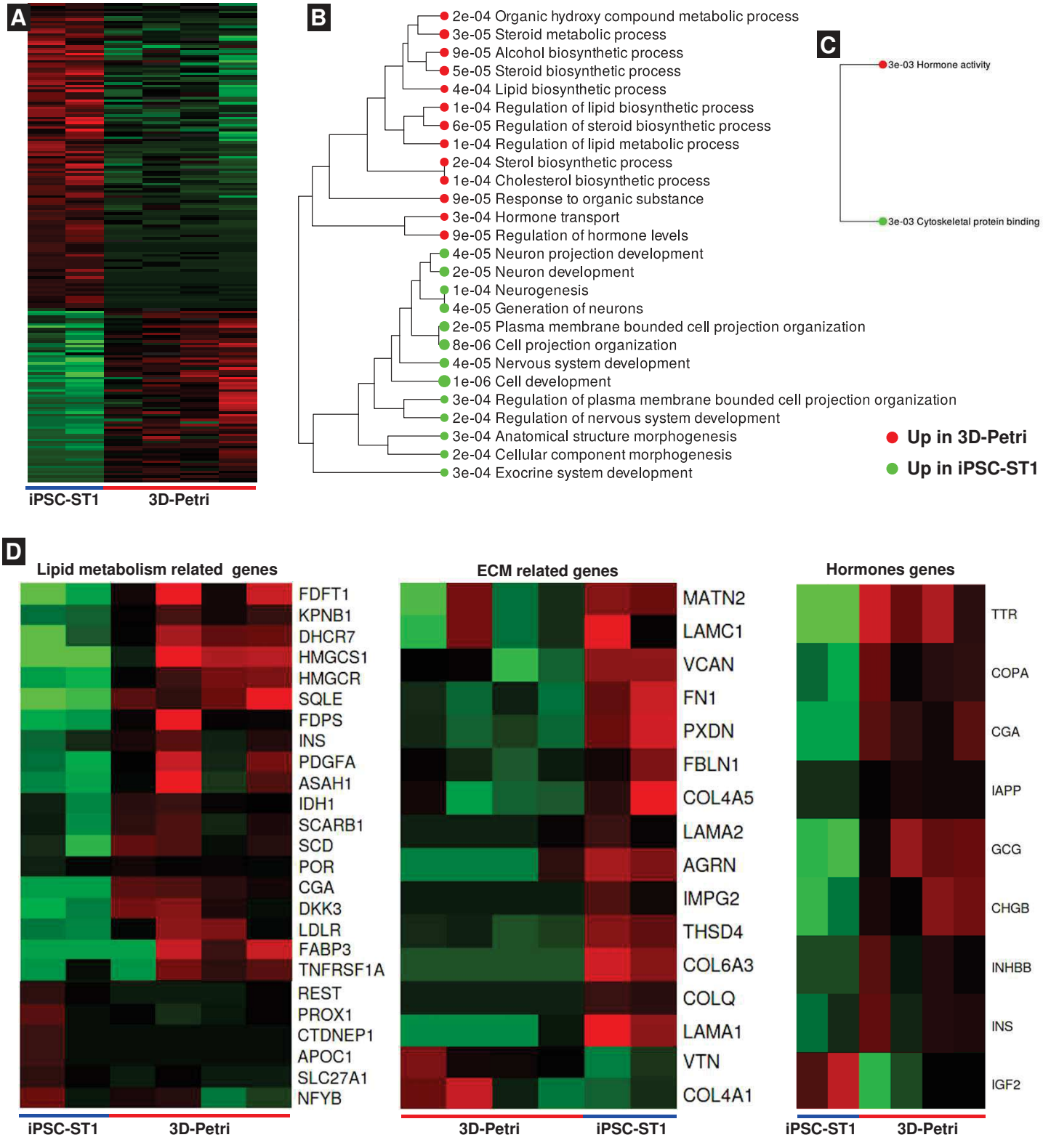
A
iPSC-ST1
3D-Petri
B
2e-04 Organic hydroxy compound metabolic process
3e-05 Steroid metabolic process
9e-05 Alcohol biosynthetic process
5e-05 Steroid biosynthetic process
4e-04 Lipid biosynthetic process
1e-04 Regulation of lipid biosynthetic process
6e-05 Regulation of steroid biosynthetic process
1e-04 Regulation of lipid metabolic process
2e-04 Sterol biosynthetic process
1e-04 Cholesterol biosynthetic process
9e-05 Response to organic substance
3e-04 Hormone transport
9e-05 Regulation of hormone levels
4e-05 Neuron projection development
2e-05 Neuron development
1e-04 Neurogenesis
4e-05 Generation of neurons
2e-05 Plasma membrane bounded cell projection organization
8e-06 Cell projection organization
4e-05 Nervous system development
1e-06 Cell development
3e-04 Regulation of plasma membrane bounded cell projection organization
2e-04 Regulation of nervous system development
3e-04 Anatomical structure morphogenesis
2e-04 Cellular component morphogenesis
3e-04 Exocrine system development
C
3e-03 Hormone activity
3e-03 Cytoskeletal protein binding
Up in 3D-Petri
Up in iPSC-ST1
D
Lipid metabolism related genes
FDFT1
KPNB1
DHCR7
HMGCS1
HMGCR
SQLE
FDPS
INS
PDGFA
ASAH1
IDH1
SCARB1
SCD
POR
CGA
DKK3
LDLR
FABP3
TNFRSF1A
REST
PROX1
CTDNEP1
APOC1
SLC27A1
NFYB
iPSC-ST1
3D-Petri
ECM related genes
MATN2
LAMC1
VCAN
FN1
PXDN
FBLN1
COL4A5
LAMA2
AGRN
IMPG2
THSD4
COL6A3
COLQ
LAMA1
VTN
COL4A1
3D-Petri
iPSC-ST1
Hormones genes
TTR
COPA
CGA
IAPP
GCG
CHGB
INHBB
INS
IGF2
iPSC-ST1
3D-Petri

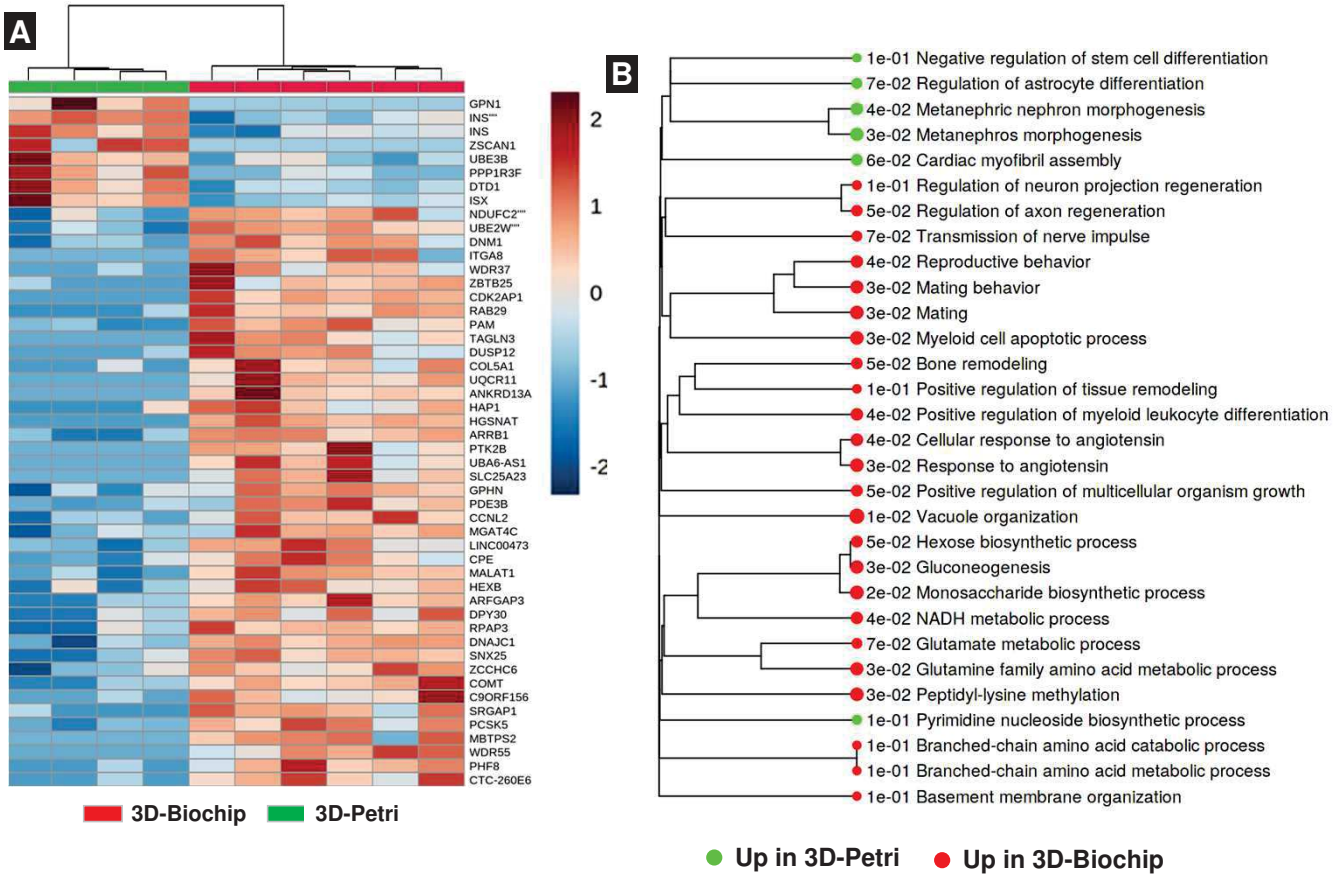
A
GPN1
INS""
INS
ZSCAN1
UBE3B
PPP1R3F
DTD1
ISX
NDUFC2""
UBE2W""
DNM1
ITGA8
WDR37
ZBTB25
CDK2AP1
RAB29
PAM
TAGLN3
DUSP12
COL5A1
UQCR11
ANKRD13A
HAP1
HGSNAT
ARRB1
PTK2B
UBA6-AS1
SLC25A23
GPHN
PDE3B
CCNL2
MGAT4C
LINC00473
CPE
MALAT1
HEXB
ARFGAP3
DPY30
RPAP3
DNAJC1
SNX25
ZCCHC6
COMT
C9ORF156
SRGAP1
PCSK5
MBTPS2
WDR55
PHF8
CTC-260E6
2
1
0
-1
-2
3D-Biochip
3D-Petri
B
1e-01 Negative regulation of stem cell differentiation
7e-02 Regulation of astrocyte differentiation
4e-02 Metanephric nephron morphogenesis
3e-02 Metanephros morphogenesis
6e-02 Cardiac myofibril assembly
1e-01 Regulation of neuron projection regeneration
5e-02 Regulation of axon regeneration
7e-02 Transmission of nerve impulse
4e-02 Reproductive behavior
3e-02 Mating behavior
3e-02 Mating
3e-02 Myeloid cell apoptotic process
5e-02 Bone remodeling
1e-01 Positive regulation of tissue remodeling
4e-02 Positive regulation of myeloid leukocyte differentiation
4e-02 Cellular response to angiotensin
3e-02 Response to angiotensin
5e-02 Positive regulation of multicellular organism growth
1e-02 Vacuole organization
5e-02 Hexose biosynthetic process
3e-02 Gluconeogenesis
2e-02 Monosaccharide biosynthetic process
4e-02 NADH metabolic process
7e-02 Glutamate metabolic process
3e-02 Glutamine family amino acid metabolic process
3e-02 Peptidyl-lysine methylation
1e-01 Pyrimidine nucleoside biosynthetic process
1e-01 Branched-chain amino acid catabolic process
1e-01 Branched-chain amino acid metabolic process
1e-01 Basement membrane organization
Up in 3D-Petri
Up in 3D-Biochip
C
6e-02 Protein serine/threonine phosphatase activity
2e-02 Phosphoprotein phosphatase activity
1e-01 Protein tyrosine/serine/threonine phosphatase activity
1e-01 Calcium activated cation channel activity
1e-01 Proteoglycan binding
2e-03 Ras GTPase binding
2e-03 Small GTPase binding
2e-03 GTPase binding
2e-02 Rab GTPase binding
6e-02 SNARE binding
4e-02 Nuclear localization sequence binding
2e-03 Ubiquitin protein ligase binding
2e-03 Ubiquitin-like protein ligase binding
2e-01 Tumor necrosis factor receptor superfamily binding
1e-01 Ubiquitin conjugating enzyme binding
1e-01 Isoprenoid binding
7e-02 Retinoid binding
6e-02 Monosaccharide binding
1e-01 Exoribonuclease activity
1e-01 Exoribonuclease activity, producing 5 -phosphomonoesters
5e-02 3 -5 -exoribonuclease activity
1e-01 Oxidoreductase activity, acting on the CH-CH group of donors
2e-02 Steroid dehydrogenase activity
1e-02 Ligase activity, forming carbon-nitrogen bonds
2e-02 Protein methyltransferase activity
2e-02 N-methyltransferase activity
5e-02 Protein-lysine N-methyltransferase activity
3e-02 Lysine N-methyltransferase activity
3e-02 S-adenosylmethionine-dependent methyltransferase activity
1e-01 Thyroid hormone receptor binding

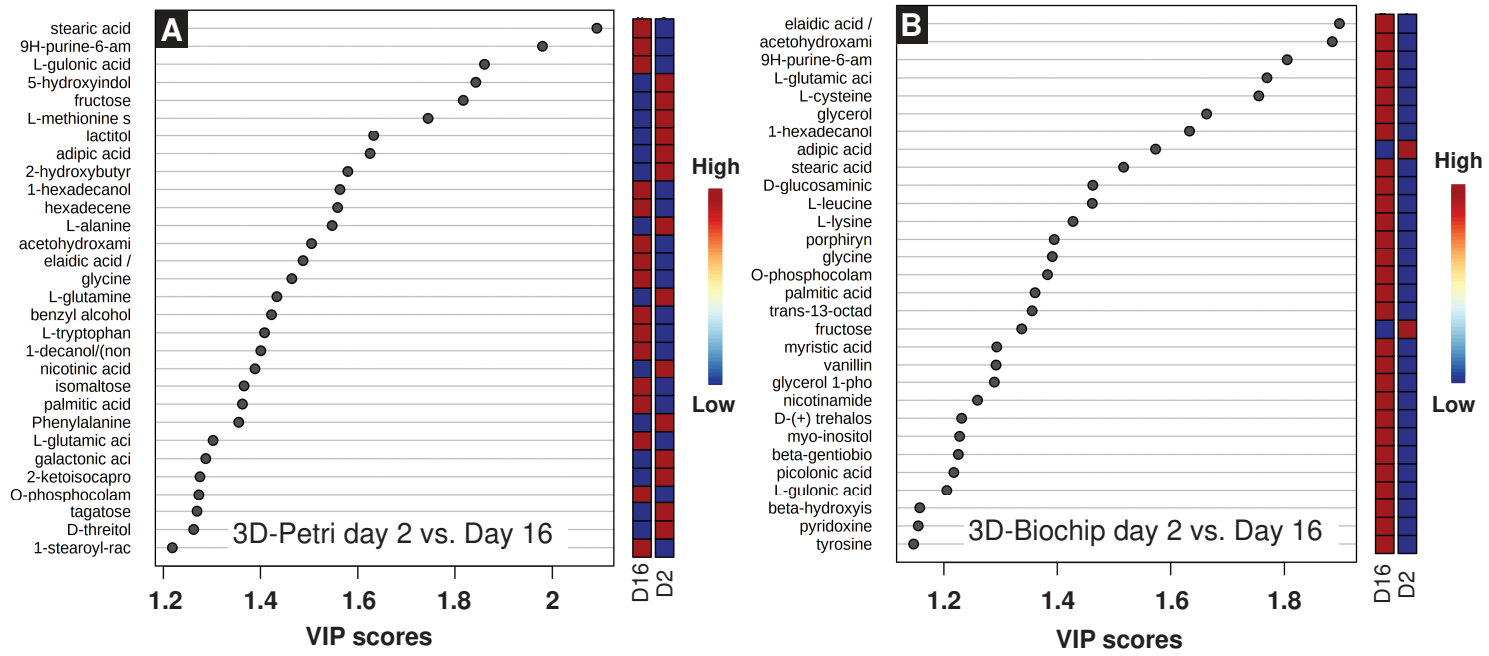
A
stearic acid
9H-purine-6-am
L-gulonic acid
5-hydroxyindol
fructose
L-methionine s
lactitol
adipic acid
2-hydroxybutyr
1-hexadecanol
hexadecene
L-alanine
acetohydroxami
elaidic acid /
glycine
L-glutamine
benzyl alcohol
L-tryptophan
1-decanol/(non
nicotinic acid
isomaltose
palmitic acid
Phenylalanine
L-glutamic aci
galactonic aci
2-ketoisocapro
O-phosphocolam
tagatose
D-threitol
1-stearoyl-rac
3D-Petri day 2 vs. Day 16
1.2
1.4
1.6
1.8
2
VIP scores
High
Low
D16
D2
B
elaidic acid /
acetohydroxami
9H-purine-6-am
L-glutamic aci
L-cysteine
glycerol
1-hexadecanol
adipic acid
stearic acid
D-glucosaminic
L-leucine
L-lysine
porphiryn
glycine
O-phosphocolam
palmitic acid
trans-13-octad
fructose
myristic acid
vanillin
glycerol 1-pho
nicotinamide
D-(+) trehalos
myo-inositol
beta-gentiobio
picolonic acid
L-gulonic acid
beta-hydroxyis
pyridoxine
tyrosine
3D-Biochip day 2 vs. Day 16
1.2
1.4
1.6
1.8
VIP scores
High
Low
D16
D2

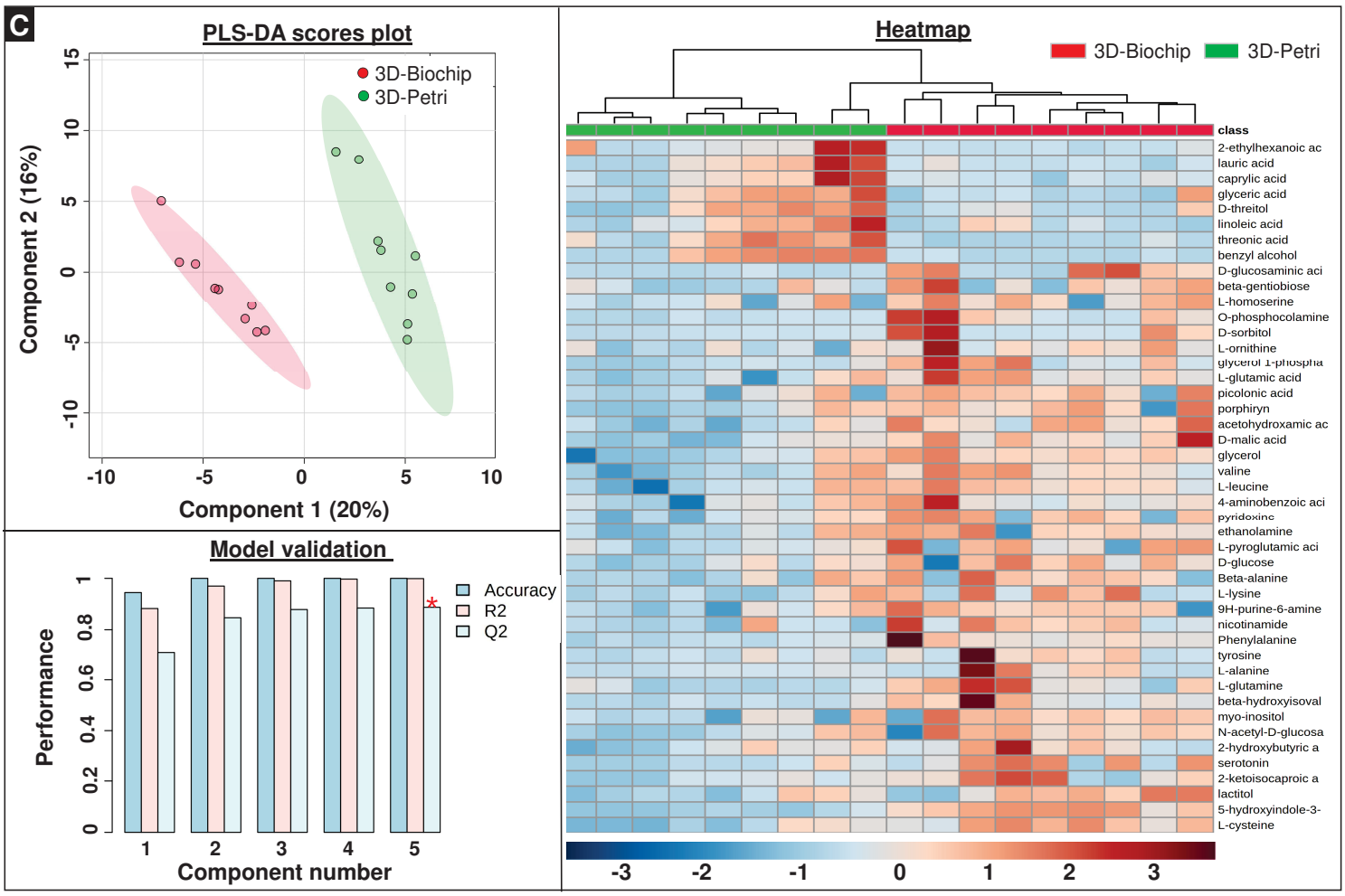
C
PLS-DA scores plot
3D-Biochip
3D-Petri
Component 2 (16%)
Component 1 (20%)
Model validation
Accuracy
R2
Q2
Performance
Component number
Heatmap
3D-Biochip
3D-Petri
class
2-ethylhexanoic ac
lauric acid
caprylic acid
glyceric acid
D-threitol
linoleic acid
threonic acid
benzyl alcohol
D-glucosaminic aci
beta-gentiobiose
L-homoserine
O-phosphocolamine
D-sorbitol
L-ornithine
L-glutamic acid
picolonic acid
porphiryn
acetohydroxamic ac
D-malic acid
glycerol
valine
L-leucine
4-aminobenzoic aci
ethanolamine
L-pyroglutamic aci
D-glucose
Beta-alanine
L-lysine
9H-purine-6-amine
nicotinamide
Phenylalanine
tyrosine
L-alanine
L-glutamine
beta-hydroxyisoval
myo-inositol
N-acetyl-D-glucosa
2-hydroxybutyric a
serotonin
2-ketoisocaproic a
lactitol
5-hydroxyindole-3-
L-cysteine

Supplementary file 1

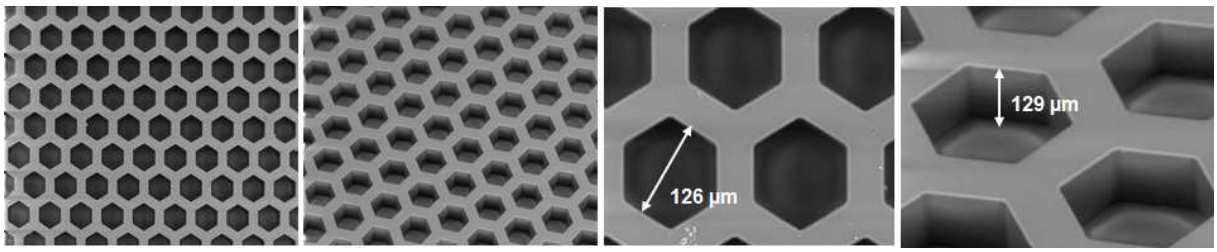

Fig.S1. Design and structure of honeycomb used for hiPSC derived β-cells spheroids formation and cultures. View from Scanning Electronic Microscope (SEM).

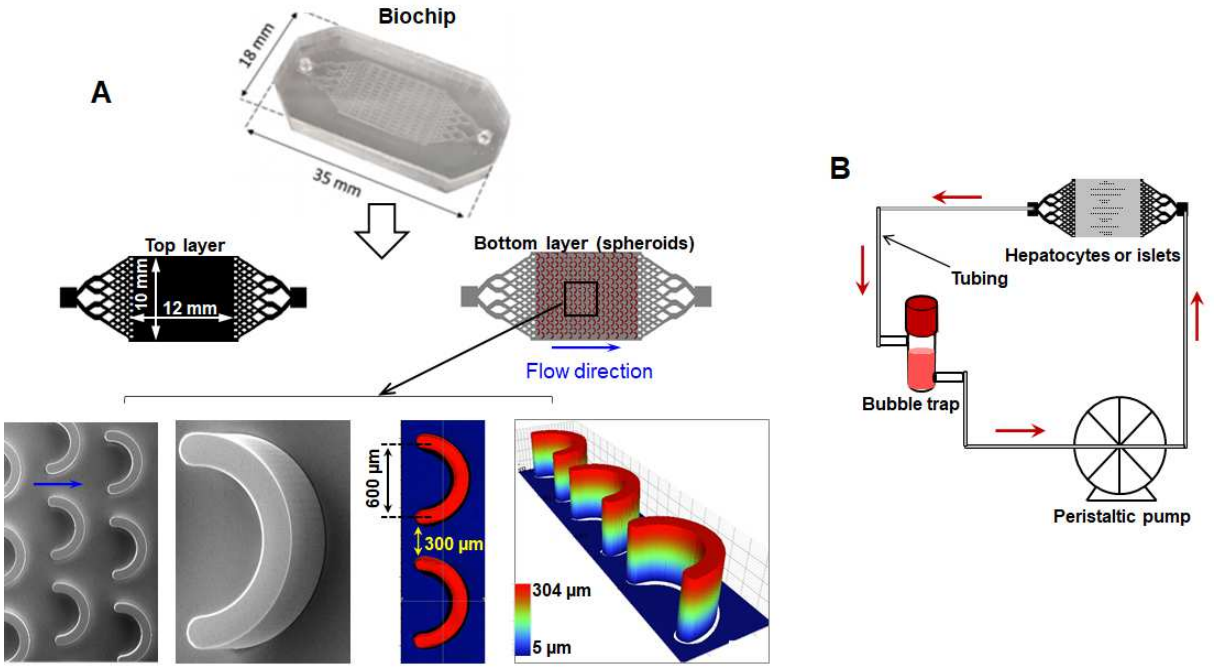

Fig.S2. (A) Design and dimensions of biochips used for hiPSC derived β-cells spheroids cultures and (B) setup used for dynamic culture in biochips.

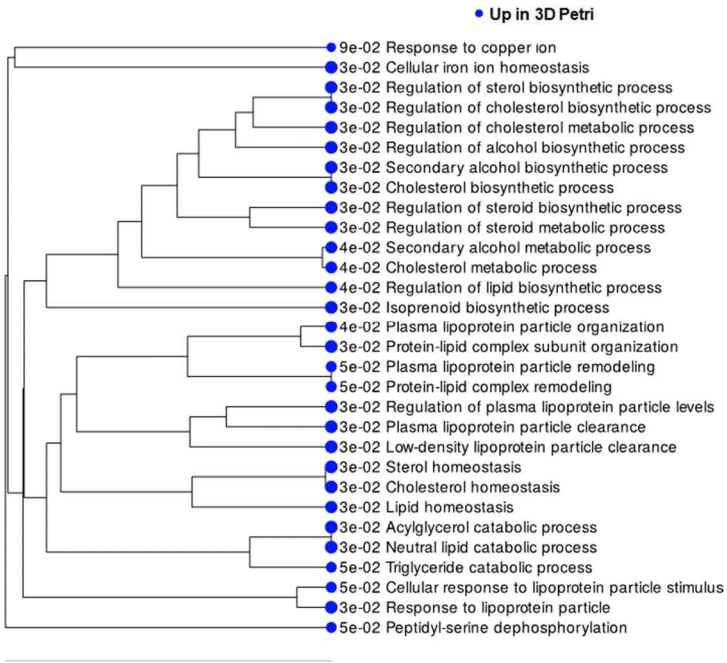

Fig.S3. GO_biological_process pathways identified by Gene Set Enrichment Analysis (GSEA) method (3D petri vs. iPSCs stage 1 comparison).

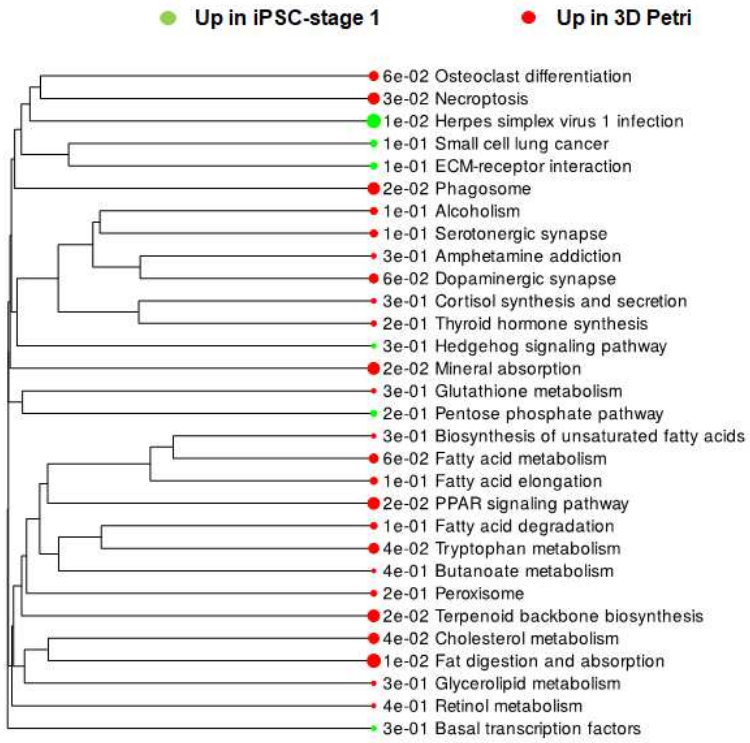

Fig.S4. GO_KEGG pathways identified by Gene Set Enrichment Analysis (GSEA) method (3D petri vs. iPSCs stage 1 comparison).

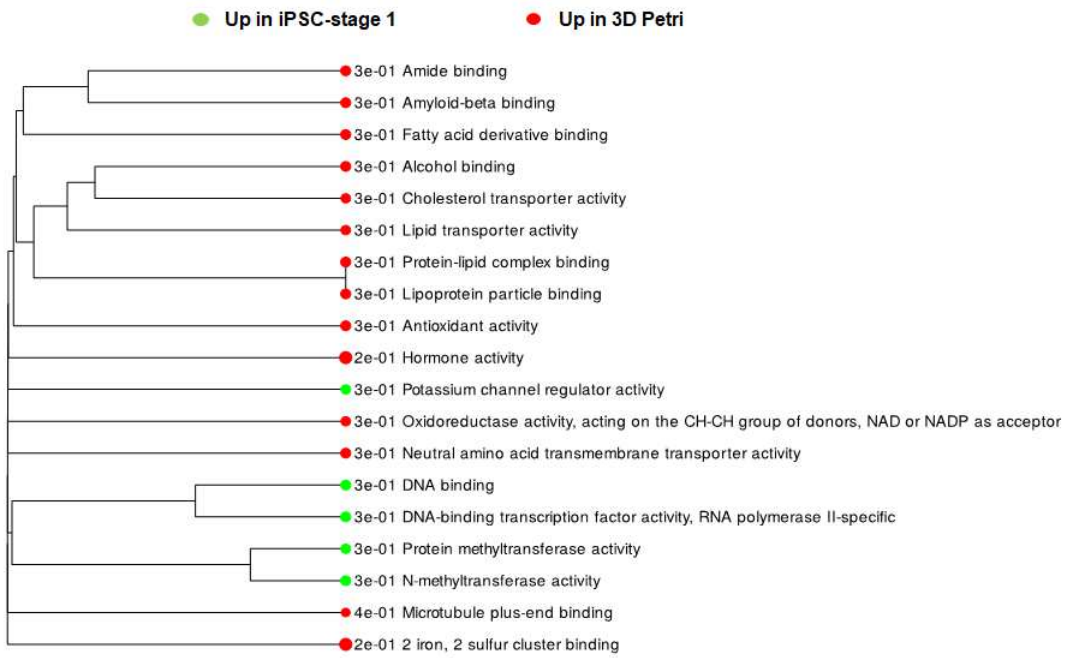

Fig.S5. GO_molecular_functions identified by Gene Set Enrichment Analysis (GSEA) method (3D petri vs. iPSCs stage 1 comparison).

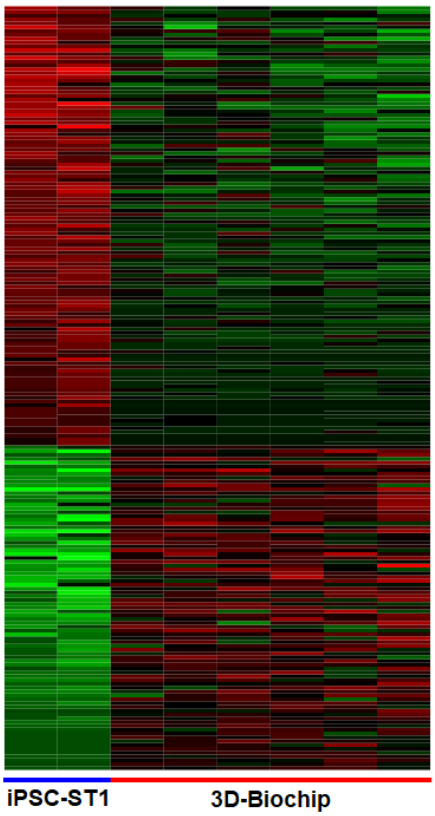

Fig.S6. Heatmap illustrating the transcriptomic separation (418 genes, 185 upregulated in biochip; 233 upregulated in stage 1 iPSC) of the 3D Biochip (spheroids at the end of the cultures) and stage 1 iPSC conditions (red upregulated, green downregulated). The list of genes is given in Supplementary file 5. Among them TTR, GCG, IAPP, CGA, CHGB, HIF3A, ACAT2, HMGCS1, PLIN2, APOB, SQLE were upregulated in 3D biochips.

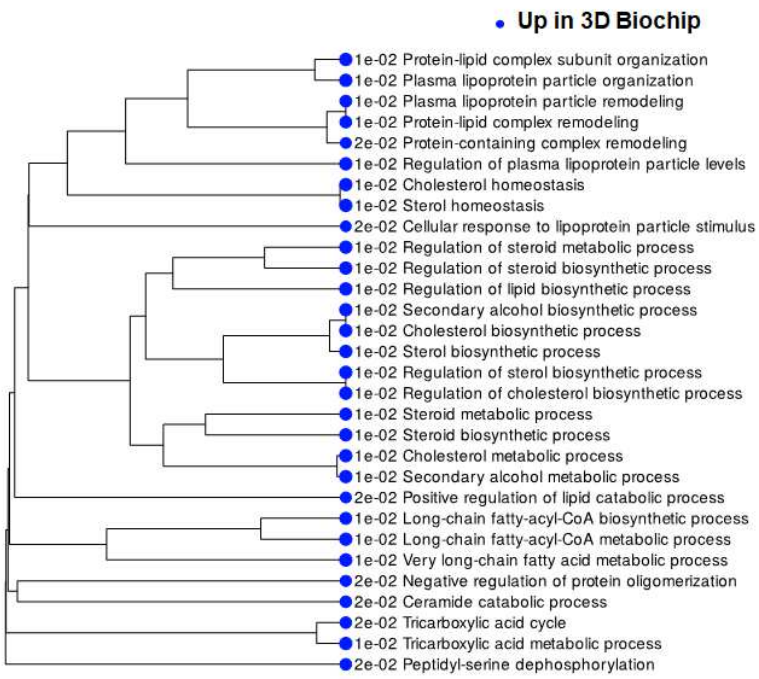

Fig.S7. GO_biological_process pathways identified by Gene Set Enrichment Analysis (GSEA) method (3D Biochip vs. iPSCs stage 1 comparison).

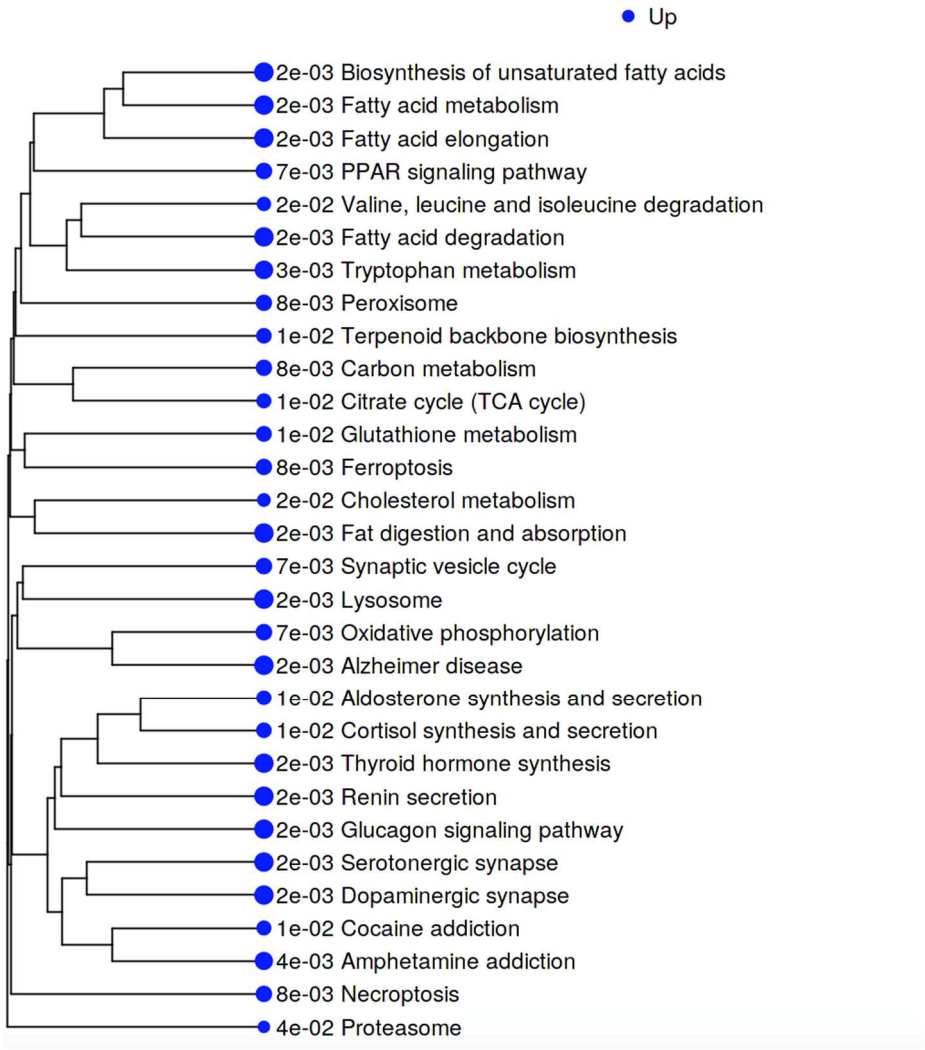

Fig.S8. GO_KEGG pathways identified by Gene Set Enrichment Analysis (GSEA) method (3D Biochip vs. iPSCs stage 1 comparison).

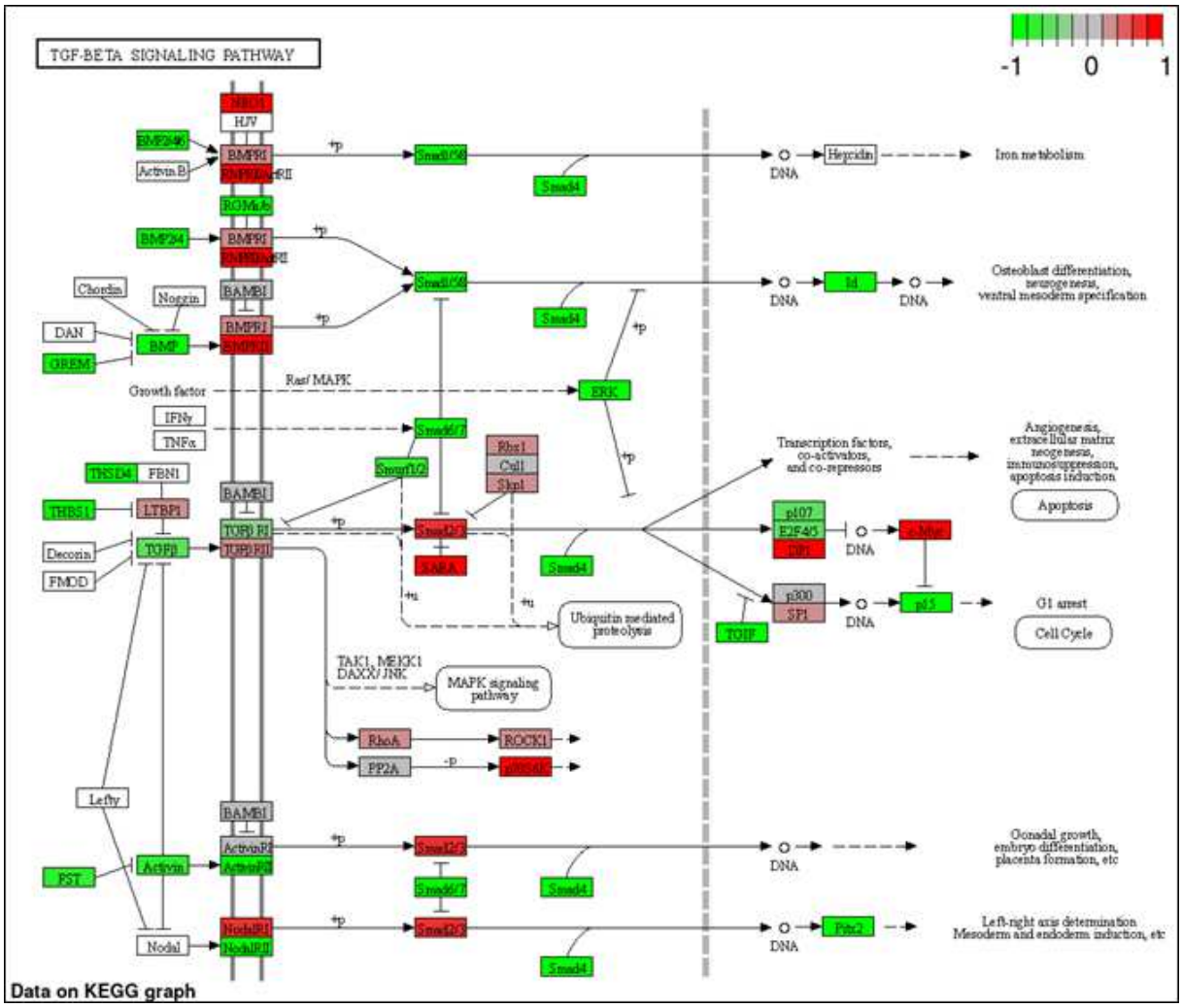

Fig.S9. Comparison of the transcriptomes of 3D biochips and 3D Petri cultures: genes significantly modulated in TGFβ signaling pathway highlighted by KEGG pathways analysis. Genes upregulated in biochips are highlighted in red, while those upregulated in 3D Petri are highlighted in green.

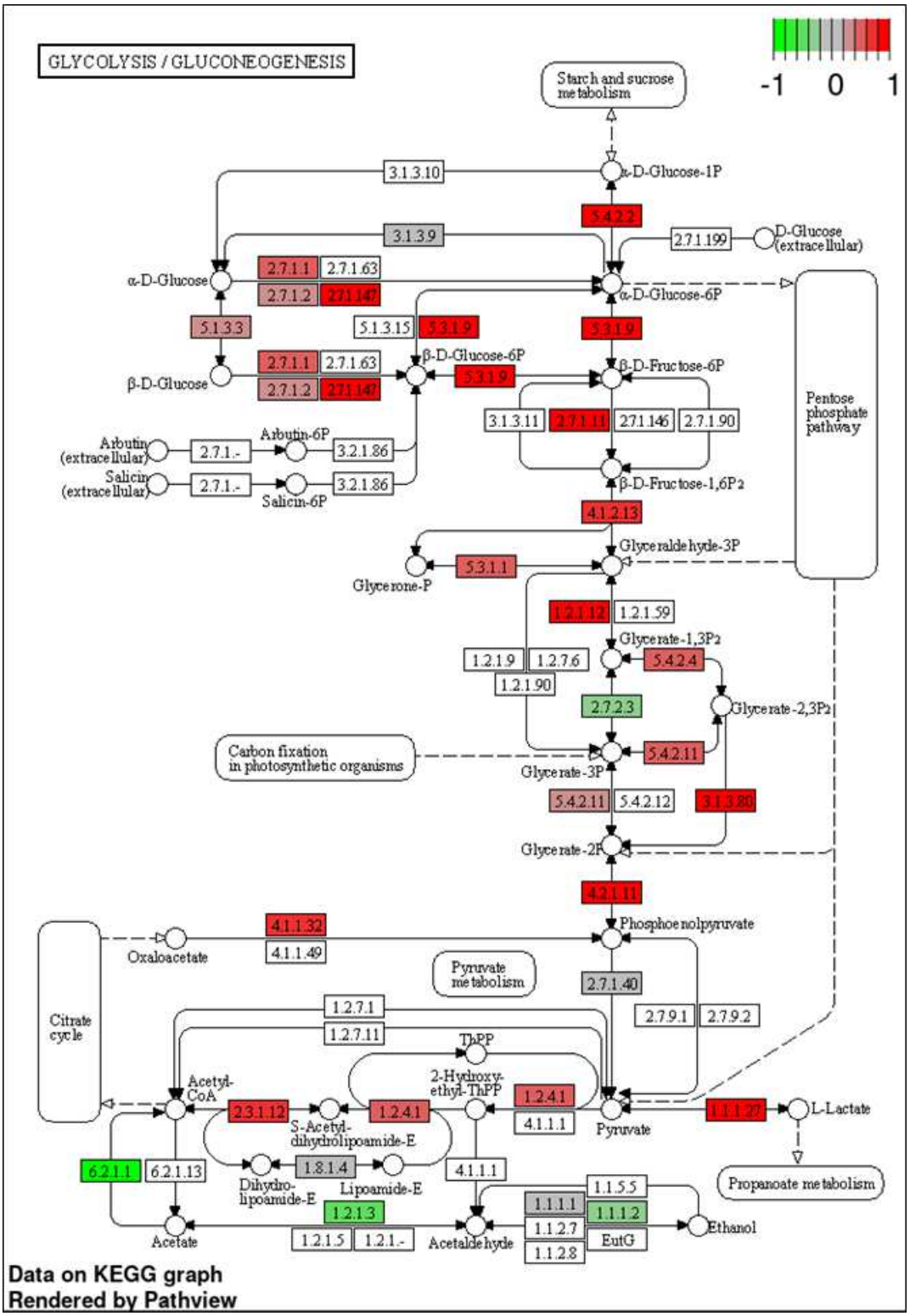

Fig.S10. Comparison of the transcriptomes of 3D biochips and 3D Petri cultures: genes significantly modulated in glycolysis/gluconeogenesis highlighted by KEGG pathways analysis. Genes upregulated in biochips are highlighted in red, while those upregulated in 3D Petri are highlighted in green.

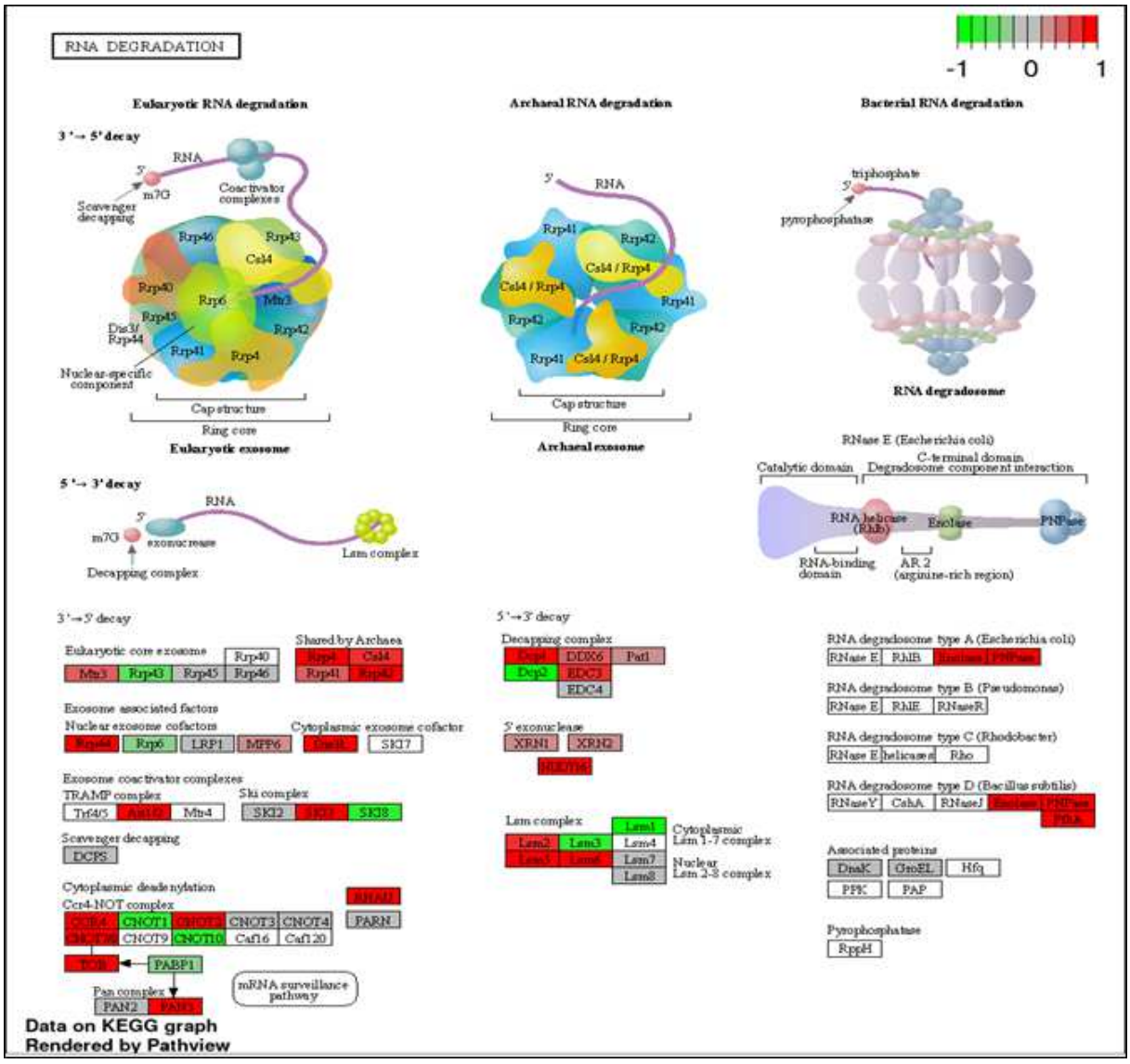

Fig.S11. Comparison of the transcriptomes of 3D biochips and 3D Petri cultures: genes significantly modulated in RNA degradation pathway highlighted by KEGG pathways analysis. Genes upregulated in biochips are highlighted in red, while those upregulated in 3D Petri are highlighted in green.

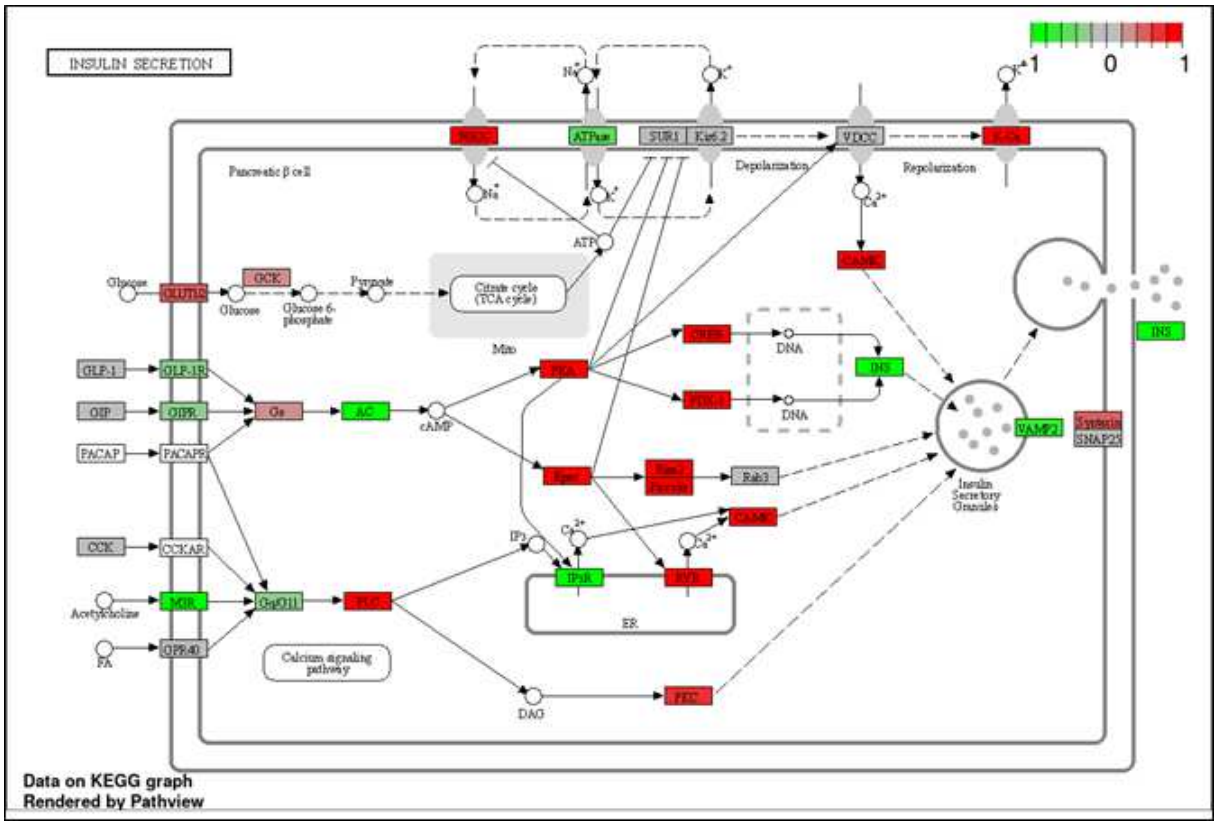

Fig.S12. Comparison of the transcriptomes of 3D biochips and 3D Petri cultures: genes significantly modulated in insulin pathway highlighted by KEGG pathways analysis. Genes upregulated in biochips are highlighted in red, while those upregulated in 3D Petri are highlighted in green.

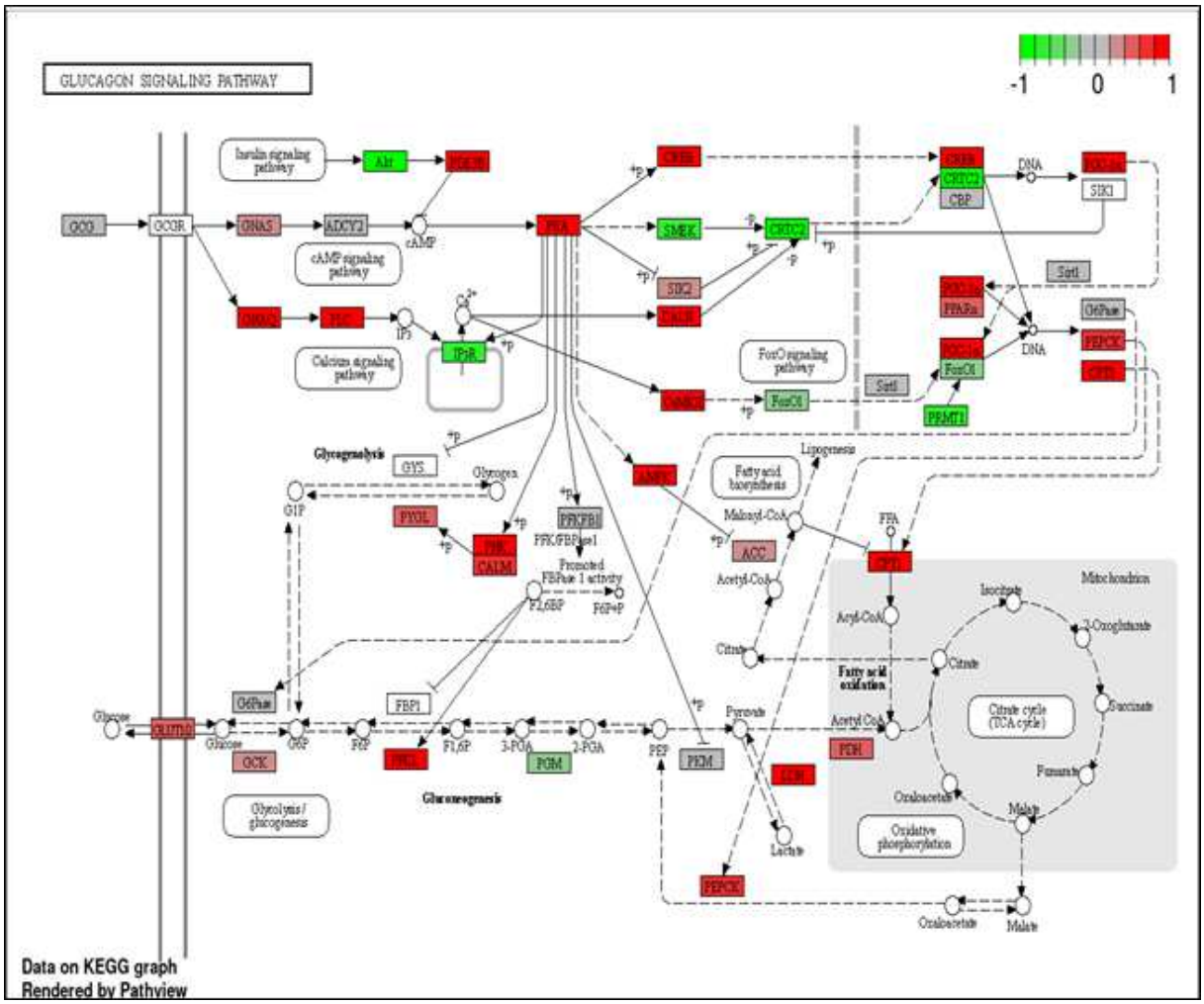

Fig.S13. Comparison of the transcriptomes of 3D biochips and 3D Petri cultures: genes significantly modulated in glucagon signaling pathway highlighted by KEGG pathways analysis. Genes upregulated in biochips are highlighted in red, while those upregulated in 3D Petri are highlighted in green.

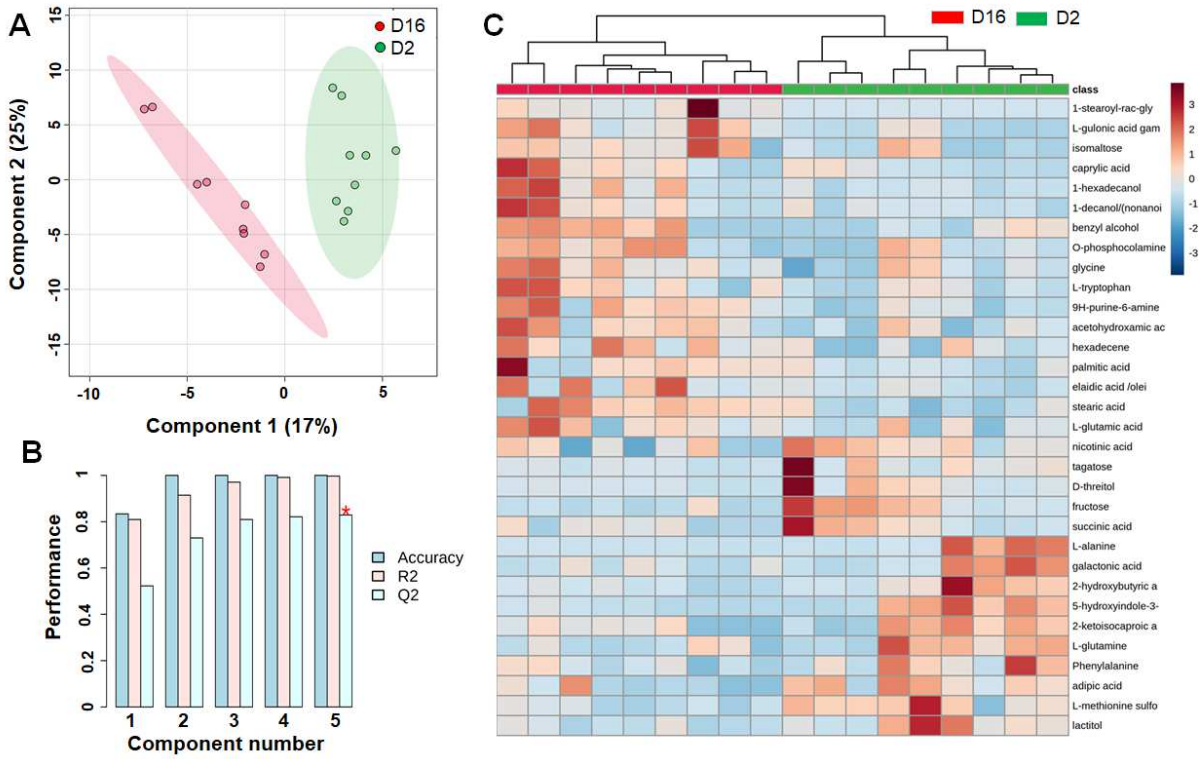

Fig.S14. Comparison of metabolomic profiles of 3D Petri cultures at day 2 and day 16. (A) PLS-DA score plot separating the two conditions; (B) PLS-DA model validation (R^2 and Q^2 > 0.5 confirming the good predictability of the model); (C) heatmap of metabolites significantly modulated between the two conditions.

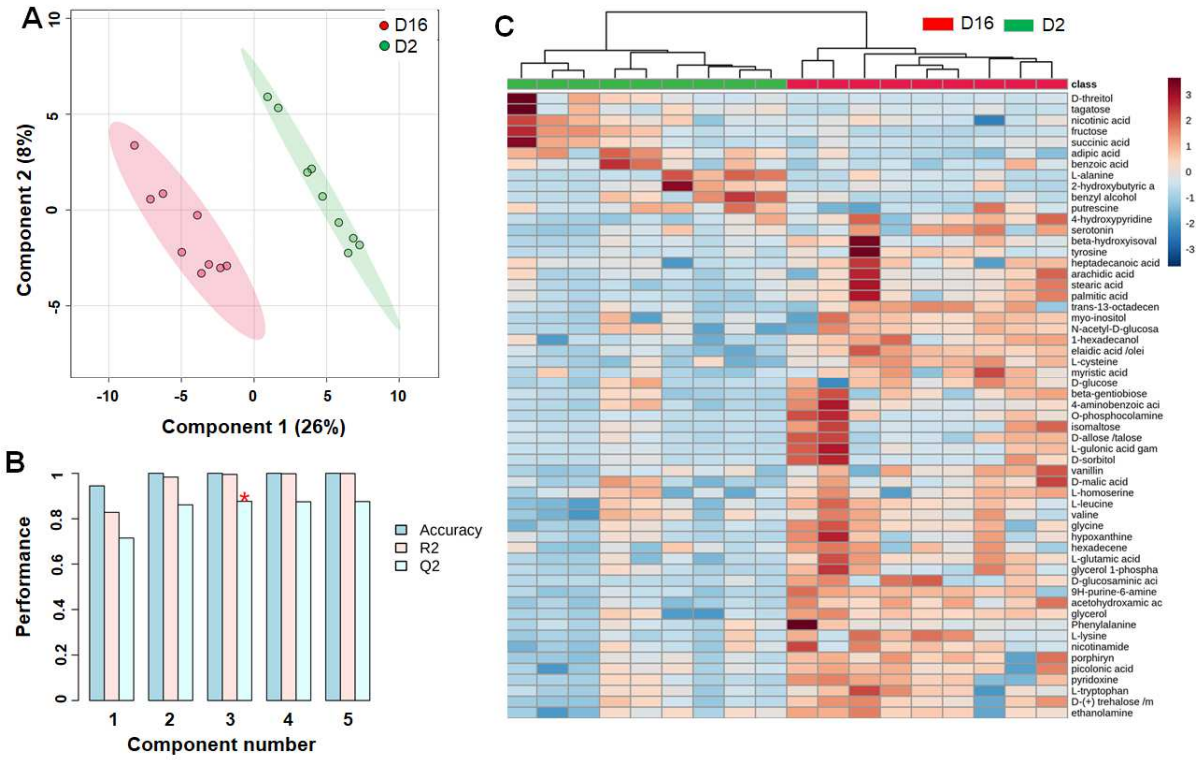

Fig.S15. Comparison of metabolomic profiles of 3D Biochip cultures at day 2 and day 16. (A) PLS-DA score plot separating the two conditions; (B) PLS-DA model validation (R^2 and Q^2 > 0.5 confirming the good predictability of the model); (C) heatmap of metabolites significantly modulated between the two conditions.

Supplementary File 2

1. Honeycomb technology

A silicon mold was fabricated using SU-8-based negative photolithography (MicroChem, Newton, MA, USA) on a silicon wafer to make honeycomb microwells (diameter: 126 µm; depth: 148 µm) and the surface was coated with CHF3, as previously described.[1] PDMS prepolymer and curing agent (Silpot 184, Dow Corning Toray, Tokyo, Japan) were mixed at 10:1 (w/w), poured onto the silicon mold and cured at 70℃ for at least 2 hours. 15 mm-diameter rounds were cut from the PDMS microwell to fit the 24-well tissue culture plate.

2. RT-qPCR assays

At the end of the experiments, 500 µl of Trizol™ Reagent (Life Technologies) were added in each biochip/well and cells were lysed by pipetting. The Trizol solutions containing cell lysates were stored at -80℃ until use. Total RNAs were extracted and purified from the Trizol solutions using a hybrid protocol combining Trizol and the RNeasy Mini Kit (QIAGEN 74104) following the manufacturer's instructions. Briefly, 100 µL of chloroform were added to Trizol solution, vortexed and incubated 5 min at room temperature (RT). After centrifugation (15 min at 120000 g), the upper aqueous phase was collected, mixed with 250 µL of isopropyl alcohol and incubated at RT for 10 min. The RNA precipitate forms a gel-like pellet after centrifugation at 120000 g for 15 min. After supernatant removing, 1 mL of ethanol was added to RNA pellet and the solution centrifugated 5 min at 7500 g. Finally, ethanol was removed, the RNA pellet dried (air dry for 5-10 min) and 20 µL of RNase-free water were added to the RNA pellet.

The concentrations and qualities of the RNAs extracted were assessed using a BioSpec-nano (Shimadzu Scientific Instruments). Reverse-transcription into cDNA was performed from 0.5 µg of total RNA using the ReverTra Ace qPCR RT Master Mix with gDNA Remover (TOYOBO). Real-time quantitative PCR was then performed with the THUNDERBIRD SYBR qPCR Mix (TOYOBO) according to the manufacturer's protocol and a StepOnePlus Real-Time PCR system (Applied Biosystems). Primer sequences of genes are shown in Table S1. β-Actin

was used as the reference gene and hiPSCs in stage 1 of maturation (iPSC-ST1) were used as the reference sample for the normalization of gene expression data.

Table S1. Primers used in RTqPCR analysis.

Gene*	Sequences
PDX1	f_ CTTGGAAACCAACAACTATTCAC r_ ATTAAGCATTTCCCACAAACA
NKX2.2	f_ ATGTAAACGTTCTGACAACT r_ TTCCATATTTGAGAAATGTTTGC
NKX6.1	f_ TCAACAGCTGCGTGATTTTC r_ CCAAGAAGAAGCAGGACTCG
NGN3	f_ TTGCGCCGGTAGAAAGGATGAC r_ TCAGTGCCAACTCGCTCTTAGG
INS	f_ CATCAGAAGAGGCCATCAAG r_ TCTTGGGTGTGTAGAAGAAGC
GCG	f_ CAGAAGAGGTCGCCATTGTT r_ TGGCTAGCAGGTGATGTTGT
SLC30A8	f_ GAGCGCCTGCTGTATCCTG r_ TGCACAAAAGCAGCTCTGAC
MAFA	f_ GTCAGCAAGGAGGAGGTGATC r_ TCACCAACTTCTCGTATTTCTCCT
GLUT2	f_ TGGGCTGAGGAAGAGACTGT r_ CCCATCAAGAGAGCTCCAACT
GCK	f_ CACTGCTGAGATGCTCTTCGAC r_ CCACGACATTGTTCCCTTCTG
SST	f_ CCCAGACTCCGTCAGTTTCTG r_ TCATTCTCCGTCTGGTTGGGT
PCSK1	f_ TGATCCCACAAACGAGAACAAAC r_ TGTGATTATTTGCTTGCATGGCA
UCN3	f_ GGCCTCCCCCACAAGTTCT r_ TCTCTTTGCCCTCCTCCTCC
PTF1A	f_ ATAGAAAACGAACCACCATTTGAGT r_ CAGGACGTTTTCTGGCCAGA
B_actin	f_ CCTCATGAAGATCCTCACCGA r_ TTGCCAATGGTGATGACCTGG

**PDX1*: pancreatic and duodenal homeobox 1 ; *NKX2.2* : NK2 homeobox 2 ; *NKS6.1* : NK6 homeobox 1 ; *NGN3* : neurogenin 3 ; *INS* : insulin ; *GCG* : glucagon ; *SLC30A8* : solute carrier family 30 member 8 ; *MAFA* : MAF bZIP transcription factor A ; *GLUT2* : solute carrier family 2 member 2 ; *GCK* : glucokinase ; *SST* : somatostatin ; *PCSK1* : proprotein convertase subtilisin/kexin type 1 ; *UCN3* : urocortin 3 ; *PTF1A* : pancreas associated transcription factor 1a.

3. Immunostaining

After transfer to an untreated TCPS 24-well plate, the spheroids were washed with phosphate buffer saline solution (PBS) and fixed in paraformaldehyde 4% at 4°C overnight. In order to perform the immunohistochemistry (IHC) staining in a 3D structure, the spheroids were permeabilized with 1% Triton X100 in PBS for 3 hours at 4°C and washed 3 times with PBS for 30 min. Then, the spheroids were blocked with a gelatin buffer for 24 hours at 4°C. Primary antibodies (Table S2) were incubated for 24 hours at 4°C in a BSA/PBS solution. After washing with PBS, secondary antibodies (Table S2) were further incubated overnight in a BSA/PBS solution at 4°C in the dark. Finally, the nuclei were stained with DAPI (342-07431, Dojindo) at 1/1000 for 30 min at room temperature (RT) in the dark. All the incubations and washing steps were carried out using a shaker. Observations were made using an Olympus IX-81 confocal laser-scanning microscope.

Table S2. Primary and secondary antibodies used for islets immunostaining*.

Immunostaining	Primary antibody	Secondary antibody
Insulin	*Mouse anti-insulin (ab6995)* ***Abcam***	*Goat anti-mouse Alexa Fluor® 594 (ab150116)* ***Abcam***
Glucagon	*Sheep anti-glucagon (ab 36232)* ***Abcam***	*Donkey anti-sheep Alexa Fluor 647 (ab 150179)* ***Abcam***
MAFA	*Rabbit anti-MAFA (ab26405)* ***Abcam***	*Goat Anti-rabbit Alexa Fluor® 680 (A-21109)* ***ThermoFisher***
PDX1	*Goat anti-PDX1 (ab347383)* ***Abcam***	*Donkey Anti-goat Alexa Fluor® 488 (ab150129)* ***Abcam***
GCK	*Mouse anti-GCK (sc-17819)* ***Santa Cruz***	*Donkey anti-mouse Alexa Fluor® 647 (ab150107)* ***Abcam***

* All antibodies were diluted in the range recommended by the manufacturers.

4. CAGE transcriptome profiling

NanoCAGE libraries were generated and sequenced as previously described by Poulain et al.2017.[2] Total RNAs were extracted from cell samples conserved in Trizol™ Reagent (Life

Technologies) and the PureLink RNA mini kit (ThermoFisher) following the manufacturer's instructions. Fifty nanograms of each total RNA were retrotranscribed to produce cDNA samples individually tagged by specific barcode sequences. Samples were subsequently PCR-amplified and multiplexed to produce a nanoCAGE library that was sequenced paired-end (9.1 pM + 10% PhiX) on a MiSeq system with the reagent kit v3 150-cycles (Illumina).

NanoCAGE sequencing data (FASTQ files) were subsequently processed for CAGEscan analysis with the cagescan-pipeline workflow (https://gitlab.com/mcfrith/cagescan-pipeline and https://github.com/oist/plessy_CAGEscan_Nextflow).[3] Briefly, Tagdust v2.33 was used to demutiplex the sequencing reads and filter out reads originating from ribosomal RNA or oligo-artifacts.[4] Remaining reads were then aligned on the human genome (hg19 and hg38) with LAST (https://gitlab.com/mcfrith/last).[5] Resulting .BED files were processed with custom R scripts using the CAGEr package[6] to produce gene expression tables that were uploaded online for differential gene expression (DGE) and pathway gene set enrichment (PGSEA) analysis with iDEP version 0.92 (http://bioinformatics.sdstate.edu/idep92/).[7] The EdgeR:log2(CPM+c) option was used to transform read counts for clustering. The DGE analysis was conducted with limma-voom,[8] applying a false discovery rate (FDR) cutoff of 0.2 and setting the minimum fold change to 1.1. Gene Set Enrichment Analysis (GSEA) and Pathway Gene Set Enrichment Analysis PGSEA was performed with a pathway significance cutoff set at 0.2. The ISMARA webserver (https://ismara.unibas.ch/mara/) was used for Motif Activity Response Analysis (MARA).[9] MetaboAnalyst 4.0 was used to perform multivariate data analysis with the transcription factor motif activity matrix extracted from ISMARA.[10]

5. Metabolomic analysis

The collected culture medium (250 µL) was completed with 500 µL of frozen solution (-20°C) of water:acetonitrile:isopropanol (2:3:3) containing 4 mg/L of adonitol, 2.75 mg/L of α-aminobutyric acid solution (αABA), and placed in an eppendorf thermomixer for 10 min at 4°C with shaking at 1500 rpm. Insoluble material was removed by two centrifugations steps at

14000 rpm for 10 min. Three aliquots of each extract (100 µL) were dried for 4 h at 35 °C in a speed-vac and stored at -80°C until analysis.

For GC-MS injection, samples were taken out of -80°C, warmed for 15 min and dried again for 1.5 h at 35 °C before adding 10 µL of 20 mg/mL methoxyamine in pyridine and the reaction was performed for 90 min at 30 °C with shaking. Then, 90 µL of N-methyl-N-trimethylsilyl-trifluoroacetamide (MSTFA, Regis Technologies) was added and the reaction continued for 30 min at 37 °C. After cooling, 100 µL was transferred to an Agilent vial for injection. Four hours after derivatization, 1 µL of sample was injected in splitless mode on an Agilent 7890B gas chromatograph coupled to an Agilent 5977A quadrupole mass spectrometer. The column was a Rxi-5SilMS from Restek (30 m with 10 m Integra-Guard column - ref 13623-127). An injection in split mode with a ratio of 1:30 was systematically performed for saturated compound quantification. The oven temperature ramp was 60 °C for 1 min then 10 °C/min to 325 °C for 10 min. Helium constant flow was 1.1 mL/min. Temperatures were the following: injector: 250 °C, transfer line: 290 °C, source: 230 °C and quadrupole 150 °C. The quadrupole mass spectrometer was switched on after a 5.90 min solvent delay time, scanning from 50-600 u. Samples were randomized and fatty acid methyl ester mix (C8, C9, C10, C12, C14, C16, C18, C20, C22, C24, C26, C28, C30) was injected in the middle of the queue for external RI calibration.

Raw Agilent datafiles were analyzed with AMDIS (http://chemdata.nist.gov/mass-spc/amdis/). The Agilent Fiehn GC/MS Metabolomics RTL Library (version June 2008) was employed for metabolite identifications. Peak areas were determined with the Masshunter Quantitative Analysis (Agilent) in splitless and split 30 modes. Because automated peak integration was occasionally erroneous, integration was verified manually for each compound and peak areas were normalized to ribitol. Metabolite contents are expressed in arbitrary units (semi-quantitative determination).

Specific references associated to the protocols:

1 M. Shinohara, H. Kimura, K. Montagne, K. Komori, T. Fujii and Y. Sakai, *Biotechnol. Prog.*, **2014**, 30, 178-187.

2 S. Poulain, S. Kato, O. Arnaud, J. E. Morlighem, M. Suzuki, C. Plessy and M. Harbers, in *Promoter Associated RNA. Methods in Molecular Biology*, ed. S. Napoli, Humana Press, New York, 2020, NanoCAGE: A method for the analysis of coding and noncoding 5′-capped transcriptomes, 57-109.

3 C. Plessy, N. Bertin, H. Takahashi, R. Simone, M. Salimullah, T. Lassmann, M. Vitezic, J. Severin, S. Olivarius, D. Lazarevic, N. Hornig, V. Orlando, I. Bell, H. Gao, J. Dumais, P. Kapranov, H. Wang, C. A. Davis, T. R. Gingeras, J. Kawai, C. O. Daub, Y. Hayashizaki, S. Gustincich and P. Carninci, *Nat. Methods*, 2010, **7**, 528-534.

4 T. Lassmann, *BMC Bioinformatics*, 2015, **16**, 24.

5 S. M. Kiełbasa, R. Wan, K. Sato, P. Horton and M. C. Frith, *Genome Res.*, 2011, **21**, 487-493.

6 V. Haberle, A. R. Forrest, Y. Hayashizaki, P. Carninci and B. Lenhard, *Nucleic Acids Res.*, 2015, **43**, e51.

7 S. X. Ge, E. W. Son and R. Yao, *BMC Bioinformatics*, 2018, **19**, 534.

8 C. W. Law, Y. Chen, W. Shi and g. k. Smyth, *Genome Biol.*, 2014, **15**, R29.

9 P. J. Balwierz, M. Pachkov, P. Arnold, A. J. Gruber, M. Zavolan and E. van Nimwegen, *Genome Res.*, 2014, **24**, 869-884.

10 Z. Pang, J. Chong, G. Zhou, GD. A. de Lima Morais, L. Chang, M. Barrette, C. Gauthier, P. E. Jacques, S. Li and J. Xia, *Nucleic Acids Res.,* 2021, **49**, W388-W396.